8-1-2010

A mechanistic study of strain rate sensitivity and high rate property of tendon

John Steeneck Clemmer

A MECHANISTIC STUDY OF STRAIN RATE SENSITIVITY AND HIGH RATE PROPERTY OF TENDON

By

John Steeneck Clemmer

A Thesis
Submitted to the Faculty of Mississippi State University
in Partial Fulfillment of the Requirements
for the Degree of Master of Science
in Biomedical Engineering
in the Department of Agricultural and Biological Engineering

Mississippi State, Mississippi

August 2010

A MECHANISTIC STUDY OF STRAIN RATE SENSITIVITY AND HIGH RATE PROPERTY OF TENDON

By

John Steeneck Clemmer

Approved:

Lakiesha N. Williams Assistant Professor of Biological Engineering Major Professor	Jennifer L. Wardlaw Assistant Professor of Clinical Sciences Committee Member
Jun Liao Assistant Professor of Biological Engineering Committee Member	Steve Elder Associate Professor of Biological Engineering Graduate Coordinator
Mark Horstemeyer Professor of Mechanical Engineering Committee Member	Sarah A. Rajala Professor of Electrical Engineering Dean of Bagley College of Engineering

Name: John Steeneck Clemmer

Date of Degree: August 7, 2010

Institution: Mississippi State University

Major Field: Biomedical Engineering

Major Professor: Lakiesha N. Williams

Title of Study: A MECHANISTIC STUDY OF STRAIN RATE SENSITIVITY AND HIGH RATE PROPERTY OF TENDON

Pages in Study: 63

Candidate for Degree of Master of Science

The ultrastructural mechanism for strain rate sensitivity of collagenous tissue has not been well studied at the collagen fibril level. The objective is to reveal the mechanistic contribution of the collagen fibril to strain rate sensitivity. Collagen fibrils underwent significantly greater fibril strain relative to global tissue strain at higher strain rates. A better understanding of tendon mechanisms at lower hierarchical levels would help establish a basis for future development of constitutive models and assist in tissue replacement design.

High rate mechanical property of tendon was also studied. Tendon was compressed under high strain rate (550 /s) using a polycarbonate split Hopkinson pressure bar (PSHPB). The objectives are to investigate the tissue behavior of porcine tendon at high rates. Tendon's high rate behavior was compared with brain and liver at both hydrated and dehydrated states to investigate how water content and ultrastructural affect high rate responses of soft tissues.

ACKNOWLEDGEMENTS

This material is based upon work supported by the National Nuclear Security Administration, (Department of Energy) under award number [DE-FC26-06NT42755]. The authors would like to thank Center for Advanced Vehicular Systems, Department of Defense, Southern Regional Center for Lightweight materials, Amanda Lawrence, the MSU Electron Microscope Center, Mac McCollum, Raj Prabhu, Joe Chen, Lauren Priddy, and our Department of Agricultural and Biological Engineering.

I want to thank all my committee members for the time and thought they are giving and will give to this work. I am thankful to Dr. Lakiesha Williams and Dr. Jun Liao for providing the resource and guidance to the progress and completion of my thesis research process. I am also thankful for my parents, Steve Clemmer and Kim Clemmer, for their motivation and love.

TABLE OF CONTENTS

Page

LIST OF TABLES

LIST OF FIGURES

CHAPTER I

TENDON INTRODUCTION AND BACKGROUND

Introduction

Tendons are soft connective tissue exhibiting nonlinear viscoelastic properties, with a hierarchical structure ranging from the entire tendon to fascicle to collagen fiber to collagen fibril to the collagen molecule (Fig.1)[1-4].

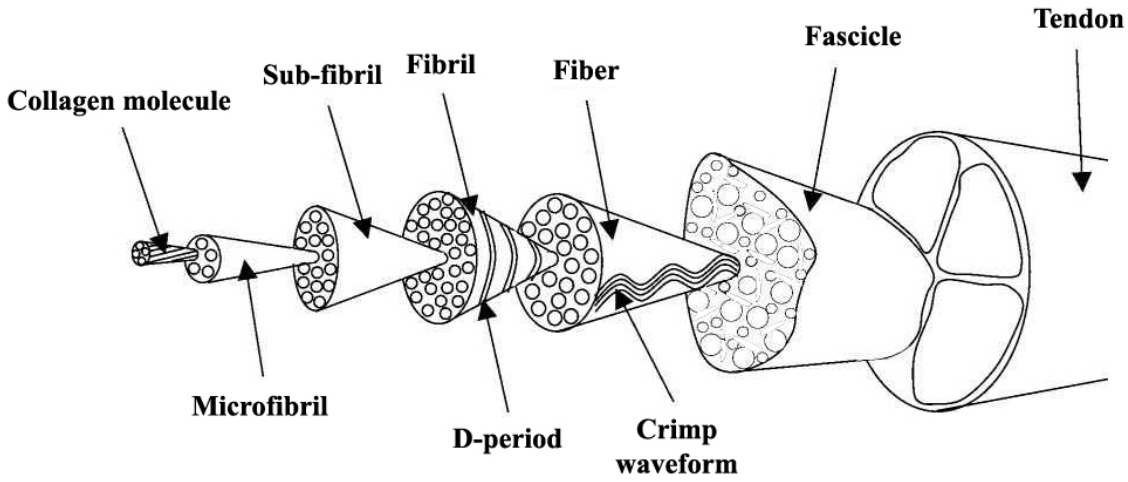

Figure 1 Tendon's hierarchical structure adopted in current study.

Notes: This schematic was adapted from Kastelic et al.[3] and Screen et al. [4].

This intricate structural hierarchy contributes to the complicated mechanical properties of tendon. Specifically, tendon shows typical viscoelastic characteristics of most soft tissues with strain rate sensitivity, stress relaxation, and creep. Many

mechanistic studies have been carried out to understand the underlying mechanisms of these viscoelastic tissue behaviors [1, 2, 5-9].

Little is known about the mechanisms behind fibrilogenisis, or the assembly of collagen molecules into fibrils, which is similar to other protein self assembly processes (such as microtubules and actin filaments.) Type I collagen fibrils are assembled in the endoplasmic reticulum of fibroblasts, although fibril formation can self-polymerize and form in the absence of cells. Cells maintain a strict control over fibrillogenesis during collagen fibril's long packing assembly [10].

Fibrils from developing tendon in chick embryos grow from their paraboloid tipped ends, with growth initially occurring all from one end and later from both[11]. The growth happens in the direction based on the collagen molecule's orientation; the N-terminal of the molecule points towards the direction of growth (creating an N-N bipolar fibril.) However, fibrils can be unipolar, having C-N terminal ends.[12]

Tendons transmit axial tensile force from muscle to bone (also capable of external compressive loads.) They are necessary for converting muscle strength into skeletal movement. Fibrils mainly run parallel with tendon's long axis, and sporadically horizontally to the longitudinal axis[13]. Tendon is surrounded by a connective tissue membrane known as epitenon which is protected by the paratenon sleeve, which minimizes friction against surrounding tissues. The fiber and lower levels are surrounded by endotenon, which contains blood vessels and nerves and provides gliding between fiber and lower hierarchies. Another structural feature of tendon is the crimping pattern seen at the fiber level[14].

The insertion site of the tendon, the osteotendinous junction, connects two very different tissues that are both highly loaded and hierarchically complicated (tendon and bone). Cooper et al. divided tendon-bone complexes into four zones[15]. The first zone is the basic tendon with fibroblasts elongated along the longitudinal axis and located between fibrils. In the second zone, cells increasingly change structure to resemble chondrocytes and fibrils start to extend into fibrocartilage. Fibrocartilage's role is to redistribute stress and inhibit any fraying of the tendon during joint movement [16]. The third zone contains mineralized fibrocartilage where crystals are present with the collagen fibrils, extending into mineral, and zone four is represented by bone.

Tendon also forms a unique bond with muscle. Collagen fibers intertwine with the ends of fibers from the muscle [17]. The sarcolemma forms pockets between fibers. The junction strength is provided by dense packing and interweaving of muscle fibers with tendon fibrils and the basal membrane ground substance as additional adhesion. The dense packing of interdigitated fibers minimizes stress concentration; and fibers mainly experience shear forces. Failure of the muscle-tendon junction usually occurs at the muscle fiber[17, 18].

Tendon Morphology

Collagen

In tendon mechanics, the central role is played by Collagen Type I, which is the major component of tendon and makes up approximately 70-80% of the tissue dry mass[19, 20]. Collagen fibril diameter distribution changes with age and affects the stiffness of tendon[21]. As the key structural protein component, the collagen molecule

consists of a triple helix formed by three poly-peptide α-chains with a length of ~300 nm and a diameter of ~1.5 nm[22]. Collagen molecules are stabilized by intermolecular linkages and covalent cross-links on their ends (by lysine, hydroxylysine, allysine, and hydroxyallysine residues)[23]. Quarter staggering of the collagen molecules gives rise to the collagen fibril with a banding appearance also known as the D-period (Fig.2) [22].

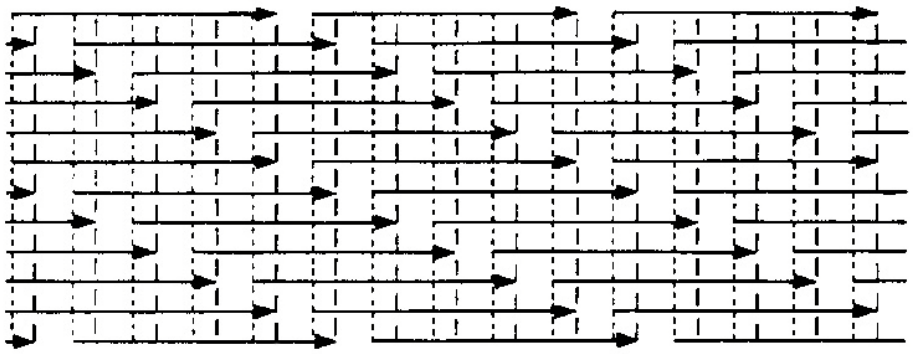

Figure 2 The Hodge Petruska model showing the collagen molecule staggering giving rise to the gap and overlapping region making up the D-period[24].

The D-period varies from 64 to 67 nm in length and is composed of a gap region and an overlapping region [25-27]. The collagen molecule in about 4.3 D-periods long, and the space between the amino and carboxy terminals of two linear molecules is approximately 0.6 of a D-period. In electron microscopic studies (scanning electron and transmission electron), the collagen D-period of tendon and ligament has been measured to be around 54 nm (analyzed within the images of the respective papers) [28-30]. This decrease in D-period length is a regular occurring effect due to the fixation process [31, 32].

Extracellular Matrix

Noncollagenous components in tendon tissue are proteoglycans, elastin, water, and fibroblasts. Elastin makes up around 2% of tendon's dry mass. Tissues that undergo high elongations and have high recovery contain more elastin. Elastin may be responsible for the recovery of the fibril crimping pattern after stretching[14]. Proteoglycans (PGs) are found in extracellular, intracellular, and cell surface locations. They are subdivided into families based on their function and characteristics. Extracellular PG's are found in numerous locations throughout the body including aorta, skeletal muscle, brain, cartilage, spine, and tendon. PGs found in tendon have a core size of 100-550 kDa or greater. PGs in tendons are aggregated by hyaluronan and have a fixed negative charge (hydrophilic)[33].

PGs control certain matrix interactions whether mechanical, structural, cellular mechanisms like adhesion, motility, proliferation, differentiation, and repair. The mechanisms that control the sequence of glycosaminoglycan (GAG) chains that is required for functional interaction is still unknown. Tendon's main PG, decorin, is a core protein that mainly interacts with fibronectin and collagen while connected to either chondroitin sulfate or dermatan sulfate, two types of GAGs [33].

Tendon's PG network is composed of highly negatively charged GAGs, which are matrix components that regulate fluid flow, attribute to viscoelasticity within the tendon [34-39], and distribute load [25, 40, 41]. GAGs are carbohydrate molecule chains that interact with several difference proteins (Fig.3). They are sulphated and negatively charged and weigh around 10-100 kDa. The two types of GAGs are non-sulphated (hyaluronic acid) and sulphated chains (chondroitin sulphate, dermatan sulphate, keratin

sulphate, heparin, and heparin sulphate. The sequence and structure of the GAG chain controls the interaction with growth factors, cell adhesion molecules, and ECM molecules, (collagen, laminin, and fibronectin)[42].

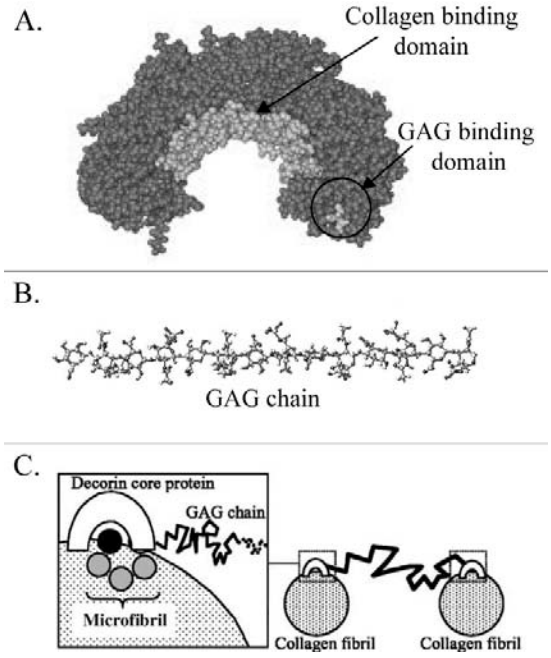

Figure 3 (A.) The decorin PG with specific collagen and GAG binding sites[43], (B.) a carbohydrate GAG chain model[25], and (C.) the PG-fibril binding complex[44] .

There has been theoretical modeling and experimental observations supporting the interfibrillar mechanical role of PG bridges [25, 40, 41] (Fig.4). Some question the noncollagenous matrix's mechanical role, stating collagen fibrils span the whole tissue and load is not transferred to PGs (GAG chains) [45]. Note that the mechanical role of PGs is still debatable and still in need of research.

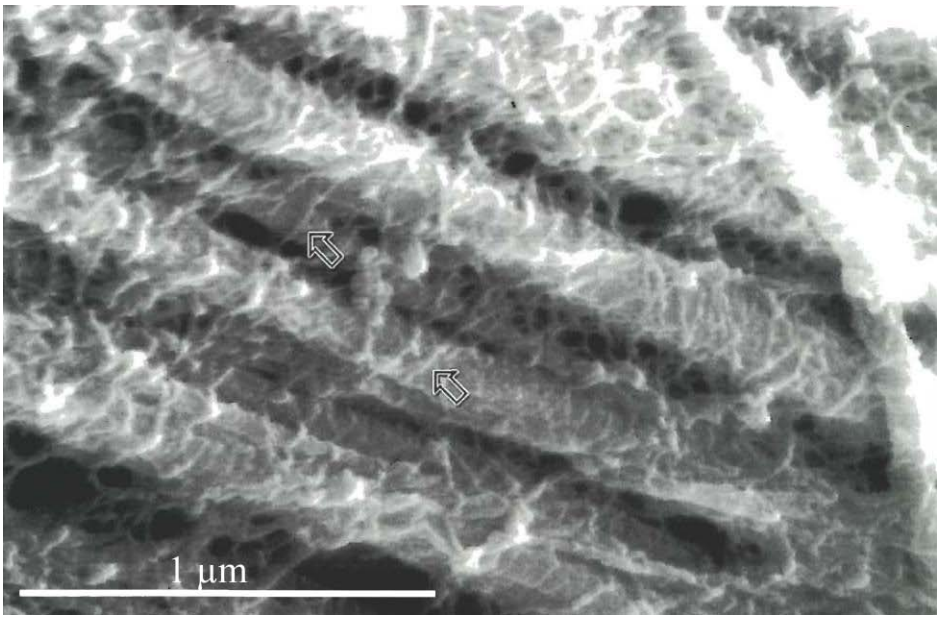

Figure 4 SEM image of collagen fibrils interwoven with PG/GAG bridges (arrows) [46].

Tendinopathic Injury

Overuse or injury of tendon tissue is a process known as tendinopathy. Physiological changes begin by fascicle disorientation [47], an increased PG and GAG content, increased water content[48], increased collagen cross-linking[49], and new vascularization [50]. Normal tendon fibrils have a bimodal diameter distribution with most fibrils being both large and small providing both high strength and flexibility (Fig.5). Tendinopathic and injured tendons contain fewer large fibrils and more small diameter fibrils while normal tendons have more large diameter fibrils which is thought to contribute to a higher tensile strength due to the high density of collagen cross-linking (Fig.6).[51]

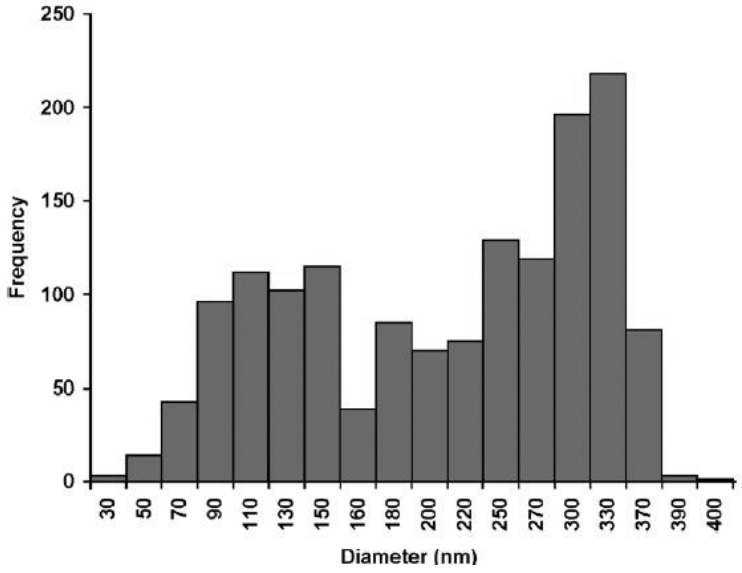

Figure 5 Typical bimodal diameter distribution of normal tendon, harvested from the proximal center of the rabbit patellar tendon[52].

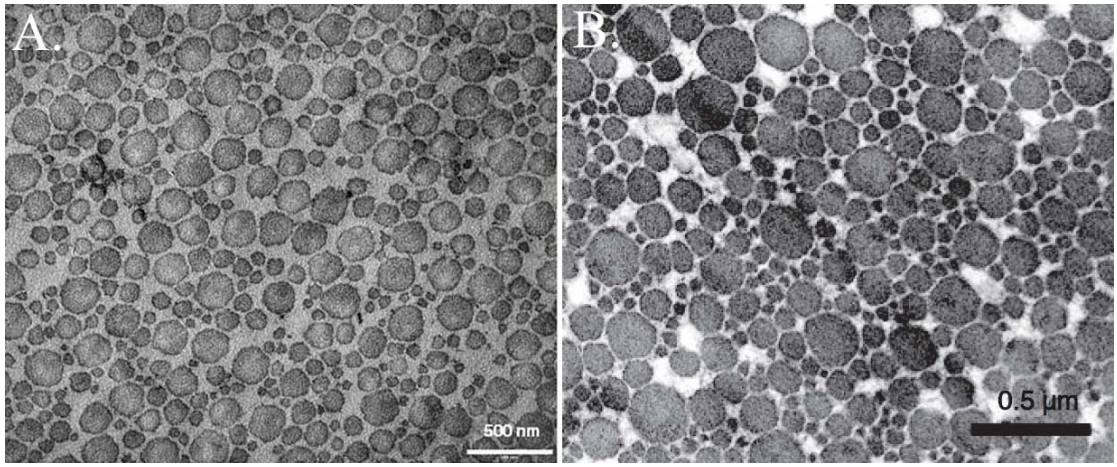

Figure 6 TEM cross section of a tendinopathic tendon[51] (A.) compared with the cross section of a normal tendon with larger fibril diameters[53] (B.) both specimen coming from human patellar tendons.

In the mechanical curve, damage occurs well before complete failure. The start of damage occurs at the fibrillar level and has been evident by relaxed fibrils and damaged matrix components[54]. New studies have shown lack of mechanical stimulation

deprives cells of stress and results in an increase in collagenase and protein synthesis in a rat model [55, 56]. This leads to a speculation that one mechanism of tendinopathy is through a catabolic pathway that is in response to the loss of strain within the cell due to isolated or damaged fibers.[57]

The steps to tendon rupture can be divided into 4 regions. The first region is a gradual concave increase of stiffness called the toe region. Applied load on the tendon elongates fibers, reducing their initial crimped morphology. Still below the elastic limit, unloading at this point results in the tendon returning to its original length and stress state. All fibers gradually get recruited in the transitional region onto the linear region of the mechanical curve. At this point, stiffness is constant as a function of strain and is considered within the physiological range of the tissue (Fig.7).

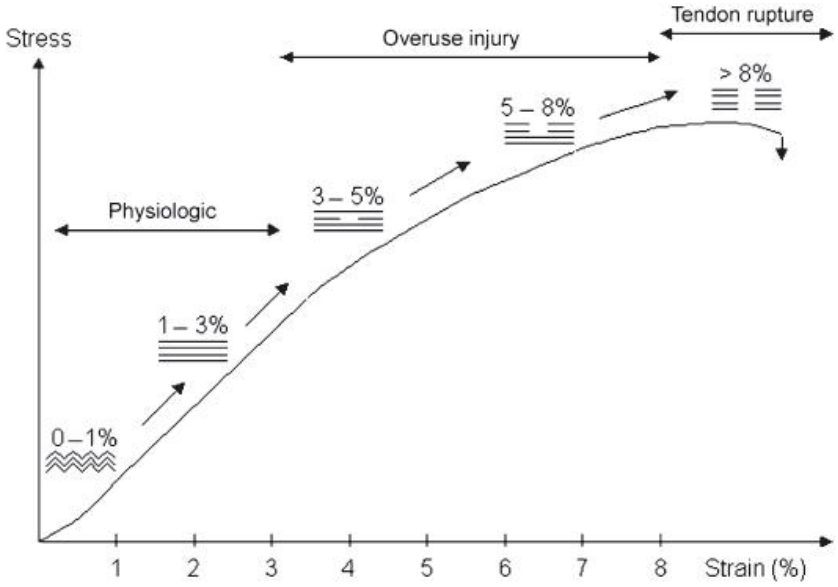

Figure 7 The typical mechanical curve of a tendon pulled to failure. Sub-failure begins to occur before complete tendon rupture[58].

Load is imposed on the fibers which are all straightened. Towards the end of the linear region, fibers gradually start to fail. This is not readily noticeable till there is a drop in stiffness. This is a "plastic deformation" in the tendon and unloading at or past this point cannot restore the original length. Strain past the "gradual failing" finally results in complete failure. Mechanical curves can differ between samples and studies due to methodological differences in clamping, strain measurements, environmental conditions, history (preserved or fresh), cross-sectional area estimation, and density (location or type of tendon[59].

Previous Studies

Yamamoto et al. is known for being one of the first to understand tendon fascicle mechanics. Yamamoto et al tested fascicles of approximately 0.3 mm diameter to investigate the differences in mechanical properties depending on location of the fascicle. There was no statistical difference in tensile properties of the 6 fascicles. Using a 1.5 %/s strain rate, fascicles were found to have a tangent modulus, tensile strength, and strain at failure of 216 ± 68 MPa, 17.2 ± 4.1 MPa, 10.9 ± 1.6 % (mean ± S.D.), respectively. Fascicles were found to have 42% tensile strength and 179% failure strain of bulk patellar tendon. Fascicles were shown to relax 29.7% compared to bulk tendon's relaxation of 51.6%, both after a 300 second stress relaxation test. Yamamoto attributes the property differences between bulk tissue and the fascicle level to ground substance contribution, collagen fibril crimping, and fascicle interaction. Yamamoto used strain rates of 0.01, 0.1, and 1%/s and fascicles were found to be strain rate sensitive. Tensile strength was shown to increase with increased strain rate. When the fascicles were tested at 1.5%/s

strain rate, the tensile strength and strain at failure were 42% and 179% of those of bulk tendon. This study reported on tensile and viscoelastic properties of rabbit patellar fascicles, showing a difference in their properties from those of bulk tendon[20].

Yamamoto also tested patellar-bone complexes and compared mechanical properties of central, lateral, and medial segments[7]. Strains were found greater at the insertion site which agrees with previous studies by Butler et al. and Kukreti et al. [28, 60, 61]. They concluded that patellar fascicles from the central portion of the tendon represent the whole patellar tendon.

Woo et al. has thoroughly investigated bulk tendon mechanics. Woo examined the mechanical properties of tendons and compared the differences in porcine flexor and extensor tendons. Flexor tendons, physiologically undergoing higher stresses and having a higher collagen concentration, were much stiffer and stronger than the extensor tendons[6]. Woo also studied how skeletal maturity impacted biomechanical properties more than strain rate effects on the ligaments in young and mature rabbits. In the skeletally immature rabbits, failure sites were found at the tibial insertion site while the mature ligaments failed in the midsubstance. Danto and Woo later conducted a study on strain rate sensitivity and mechanical properties on the anterior cruciate ligament (ACL) and patellar tendon in mature rabbits. Woo concluded a higher sensitivity to rate within the patellar tendon than the ACL, an overall 94% increase in modulus going from 0.02%/s to 135%/s strain rates[62].

Objectives

Specific Aims for Chapter II: Ultrastructural Perspective of Strain Rate Sensitivity of Tendon in Tension

The objective is to reveal the mechanistic contribution of tendon's structural components to tissue strain rate sensitivity in tension, specifically to examine the collagen fibril strain relative to global tissue strain.

1. Interruption mechanical testing (IMT) was applied at various strain rates (0.1 , 10, and 70 %/s) to the middle portion of the rabbit patellar tendon.
2. Scanning electron microscopy (SEM) was used to analyze collagen fibrils in the chemically fixed tendon fascicles that have been loaded to the same strain level at various ramping rates.
3. Image analysis was used on the SEM images to quantify fibril elongation within the midsubstance of the fascicles by determining the D-period spacing.
4. Mechanical curves were analyzed for their tangent modulus to verify strain rate sensitivity and for comparison with previous fascicle studies.

Specific Aims for Chapter III: The Mechanical Response of Tendon Under High Rate Compression With Brain and Liver Comparison

The objectives are to investigate the tissue behavior of porcine tendon at high rate impacts and compare with brain and liver to reveal underlying mechanisms using a custom Split Hopkinson Pressure Bar (SHPB).

1. Both directions (axial and transverse) and multiple loading rates were used to assess tendon's directional dependence and strain rate dependence, respectively, in high-speed impact.

2. The wet and dry tendon relationship was compared with two other soft tissues, brain and liver, in terms of stress-strain characteristics, initial hardening peak values, and ultimate stress.
3. SEM imaging of all tissues were examined to reveal the structure of three types of tissue under hydrated and dry conditions.
4. Histology was used to see morphology and distribution of cellular constitutes.

CHAPTER II

ULTRASTRUCTURAL PERSPECTIVE OF STRAIN RATE SENSITIVITY OF TENDON IN TENSION

Introduction

Previous Fibril Studies

There have been previous studies on kinematics of collagen fibrils under uniaxial loading [24, 63-69]. Tendon fibril mechanisms have been studied mainly using X-ray diffraction techniques and TEM. Increasing load has been shown to result in elongated collagen fibrils, demonstrated by an increased D-period [24, 65, 70-72]. When collagen fibrils undergo load and are recruited, the D-period elongates due to intrinsic fibril mechanisms of molecular elongation and slippage. Sasaki et al. discovered that, below 8 MPa stress, the main mechanism of collagen fibril stretch is mainly due to collagen molecule elongation; beyond 10 MPa, an increase in gap regions and molecular slippage occurs, further contributing to the fibril elongation[24]. Along with the collagen fibril strain during tension, interfibrillar slippage takes place, indirectly demonstrated by skewed proteoglycan bridges and tight packing of collagen fibrils [40, 73]. Mechanisms of stress-relaxation and creep at the fibril level have also been studied using X-ray diffraction. Studies on rat tail tendon by Folkhard et al. [70] and mitral valve leaflet by Liao et al. [73] revealed that collagen fibril elongation rapidly decreases in the beginning

of stress relaxation, and is followed by a slower decay rate for the remainder of the relaxation. Folkhard et al. and Liao et al. also reported no creep in collagen fibrils during constant tension [70, 73]. Collagen fibril cross-linking has been shown to be the main component in resisting creep [34]. Puxkandl et al. showed an increasing trend of fibril D-period elongation with an increasing strain rate by a small angle X-ray scattering study [34].

Previous Modeling

The accurate mechanistic descriptions at various hierarchical levels help model collagenous tissue behavior. The collagen molecule has been modeled using structure property relationships in attempt to describe bond breakage between alpha helices, protein interaction, and collagen's strain rate sensitivity [74, 75]. The extracellular matrix has been modeled from a fluid interaction perspective [76] and as a load transferring structure [41, 44, 77]. Recently, combining multiscale measurements (inter-fiber sliding and intra-fiber elongation along with fibril elongation), Gupta et al. created a novel multiscale model to describe how tendon distributes load between its fiber and fibril hierarchies during stress-relaxation [78]. Recently, fascicle viscoelastic models were proposed by Lucas et al. and Elliott et al [38, 79].

Justification

The ultrastructural mechanism for strain rate sensitivity of collagenous tissue has not been well studied at the collagen fibril level. A better understanding of tendon mechanisms at lower hierarchical levels can help us better to understand tissue structure-

function relation and shed light on biomimic design of tissue replacements that are optimized in strength and robustness.

Methods

Sample Preparation

Three mature Japanese white rabbits were used in this study. The actions of sacrifice and experiment were agreed upon by the Mississippi State Institutional Animal Care and Use Committee (IACUC). Each animal was sedated with an intramuscular inoculation of medetomidine (0.5 mg/kg) and ketamine (10 mg/kg). The rabbits were then humanely euthanatized via Beuthanasia solution (100mg/ml of perntabarbitol and 1 ml per 10 lbs) intravenously or by intracardiac injection. After both hind limbs were harvested using a scalpel, each limb was wrapped in gauze, soaked in hydrating PBS and stored in a sterile, sealed plastic bag. The legs were stored at -30° C until testing procedures.

Prior to testing, the legs were thawed in phosphate buffer solution (PBS) at room temperature for two hours. Three tendons were used in the study for interrupted mechanical testing and SEM analysis (D-period measurement) and three were solely devoted to interrupted testing for modulus calculation (Fig. 8). Mechanical data from the interruption testing fascicles were also used in calculating the modulus (n = 6).

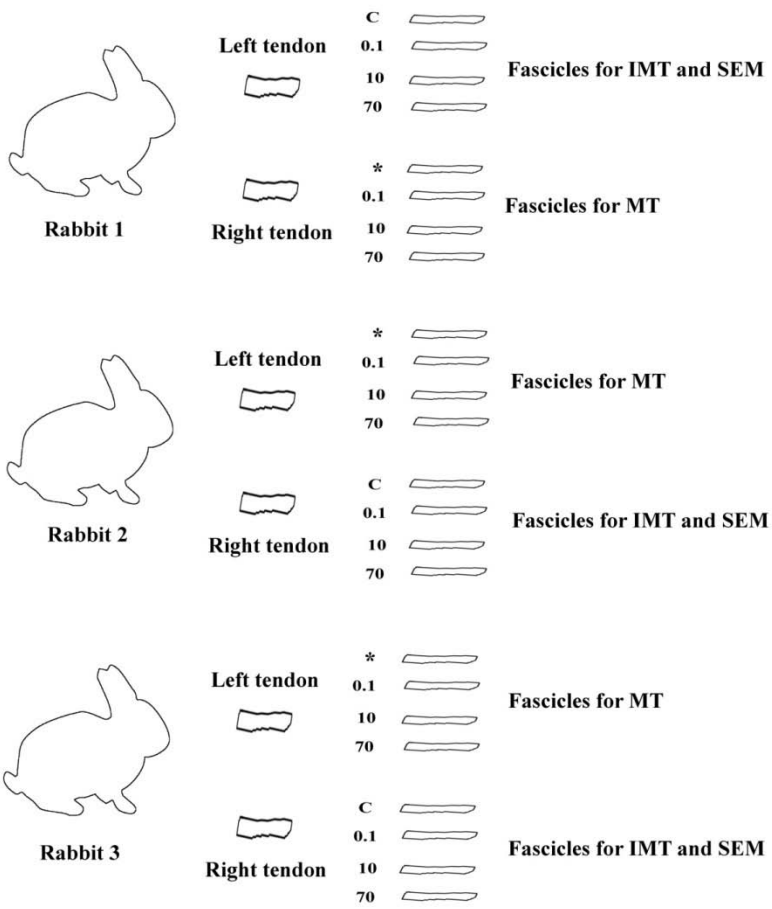

Figure 8 Number of animals and fascicles for both mechanical testing (MT) for calculations of tangent modulus and interruption mechanical testing (IMT) for calculations of D-period with SEM. Stress-strain data of IMT samples were also used for the calculation of the tangent modulus. Fascicles are labeled either control (C) or their corresponding strain rate (%/s).

Notes: *Indicates extra fascicle not used in the study.

The ends of the patellar tendon were removed and the middle portion of the tendon was carefully extracted and then trimmed into four fascicles (with the tendon kept taught). Each fascicle was cut with an approximate width of 1 mm (with the use of an electronic caliper). All fascicles used in the study were cut from the inner portions (the central 4 mm) of the tendon to prevent location variability within the tendon [52]. One

tendon from each animal yielded 4 fascicles (extracted from the inner portion of tendon), three of which were used for tensile testing and one was used as a control sample. The specimens were kept moistened with PBS during the sample extraction procedure and testing.

Interruption Tensile Mechanical Testing

Tendon fascicles were mounted onto a Biosyntech Mach-1 mechanical testing system (Mach-1™ Motion, Bio Syntech Canada, Inc, Quebec, Canada). Special grips, previously designed at CAVS testing laboratory by Stephen Horstemeyer, were used to secure the sample and minimize slippage. The fascicles were then measured for their cross-sectional areas in the midsubstance using NIH Image J digital imaging program. The average ratio of the samples' dimensions was around 7:1 (length vs. width). Fascicles were more elliptical in shape than assuming a completely round cross-sectional area. Area was defined as $A = (\pi / 4) * a * b$, where a and b are the width and depth of the fascicle.

The fascicles were preconditioned in order to give the specimens similar loading histories and reduce variation in the loading response. Each sample was preloaded at 0.01 N at 0.01 mm/s; and zero strain (gauge length) was defined at this load. Each specimen was then preconditioned to a strain of 2%, for 10 cycles at 1 Hz[20]. Control samples were subjected to the same preconditioning protocol and then fixed at a zero load in the fixative bath for the same amount of time (4 hours). From the 4 fascicles yielded from each tendon, one was used as load free control and three were loaded to 20% clamp-to-clamp strain at 0.1%/s, 10%/s, and 70%/s strain rates. This corresponded to a 12%

local strain in the midsubstance. Stress was calculated as $\sigma = F / A$, where F is force recorded by load cell and A is the cross-sectional area of the fascicle. The tangent modulus was taken from the linear portion of the curve at approximately 5% strain.

Due to the use of clamp-to-clamp control, the stress-strain data before fixation was presented as engineering stress vs. clamp-to-clamp engineering strain, in which engineering stress was calculated by normalizing force to the original cross-section of each sample, and clamp-to-clamp engineering strain was calculated by normalizing fascicle deformation to the original fascicle length at 0.01 N. Because of the inhomogeneous nature of tissue strain field from clamp-to-clamp, we monitored the local strain of midsubstance by placing two markers using permanent ink vertically on the fascicle surface and imaging the marker movement before and after the elongation[80]. The local strain was calculated by measuring the distances between the centroids of two markers.

After the interrupted tension test at the previously mentioned strain rates, a 4 oz. stand up bag (Nasco Whirl-Pak ®) was used to immerse the fascicle in 1.25% glutaraldehyde. Samples were left in the fixative bath for 4 hours before removing from the grips. The middle region of the fascicle was prepared for electron microscopy analysis (Fig.9).

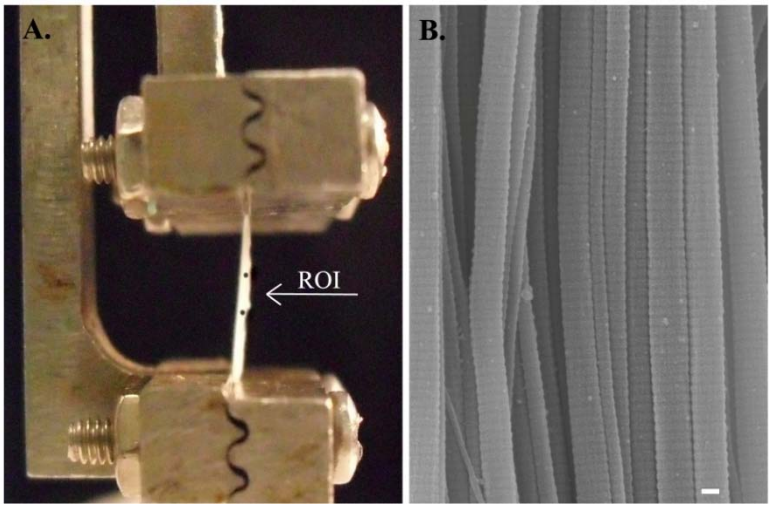

Figure 9 (A.) Fascicles were subjected to mechanical testing with 7 mm clamp-to-clamp initial length with the region of interest (ROI) between markers of 2 mm apart. (B.) Midsubstance was processed for SEM analysis for D-period measurement. Scale bar = 100 nm.

Scanning Electron Microscopy

Samples for SEM were fixed in 1.25% glutaraldehyde in 0.1 M phosphate buffer (pH 7.2), rinsed with 0.1 M phosphate buffer, and post fixed with 2% osmium tetraoxide in 0.1 M phosphate buffer. Samples were dehydrated in a graded ethanol series and then were critical point dried in a Polaron E 3000 CPD. They were then mounted on aluminum stubs and sputter coated with gold-palladium. Specimens were imaged using a JEOL JSM-6500 FE Scanning Electron Microscope.

D-period analysis

After imaging, the samples were analyzed using Image J software (Image J 1.41, National Institutes of Health, USA). SEM photographs were taken from 20,000X to 30,000X magnification. The average number of D-periods for each fibril (40 ± 9) was

averaged by Image J using the image's scale bar and a scale factor calculated by SF = (distance in pixels) / (known distance (nm)).

For each interruption tensile test, five images randomly located in the specimen's midsubstance were used to measure the fibril periodicity (Fig. 10).

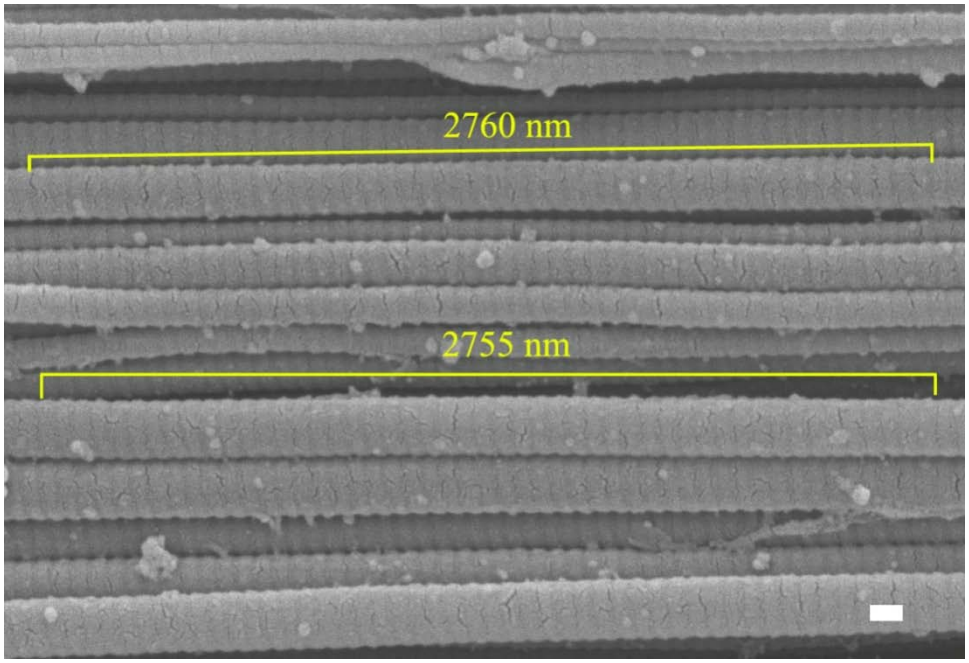

Figure 10 Image analysis for 2 fibrils after a 70%/s test. SEM image shows 50 D-periods measuring 2755 and 2760 nm (corresponding to a 55.1 nm and 55.2 nm D-period, respectively). Scale bar =100 nm.

However, in order to avoid stereological bias, in the random selection procedure one criterion was implemented, i.e., the imaging areas needed to have collagen fibrils predominately aligned along the image plane. Obviously, collagen fibrils with a large oblique orientation (out of plane) could potentially underestimate the D-period.

Six fibrils from each image were selected for D-period measurement. Again, collagen fibrils with in plane orientation were picked for an accurate measurement. The

sample size was 90 fibrils for each strain rate (Fig. 11), while the total number of fibrils analyzed for the control group was 50. This was due to the crimping nature of load free tendon and the difficulty of locating in-plane undistorted fibrils (Fig. 12-a).

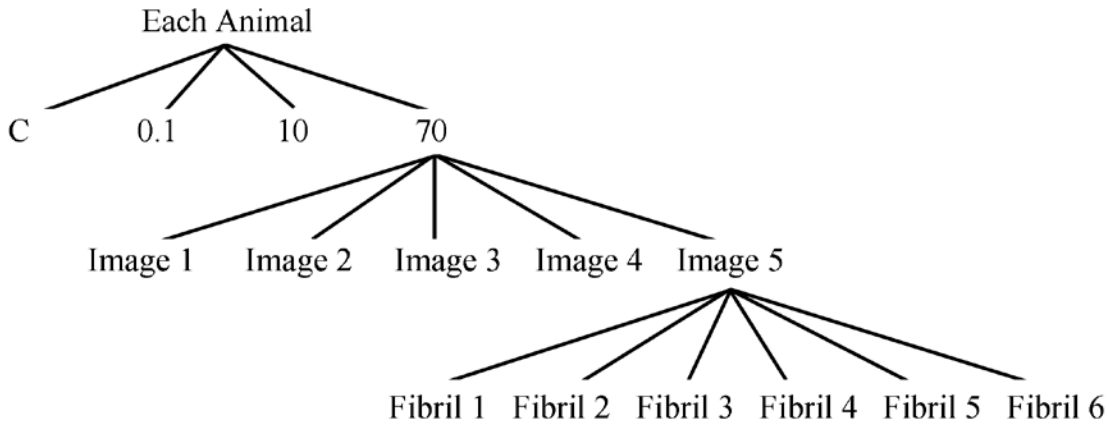

Figure 11 Sample tree for fascicles undergoing D-period analysis. A sample size of n = 90 was the total number of fibrils coming from all 3 animals (3 animals × 5 images × 6 fibrils). Each fibril measurement represented an average of 40 ± 9 D-periods.

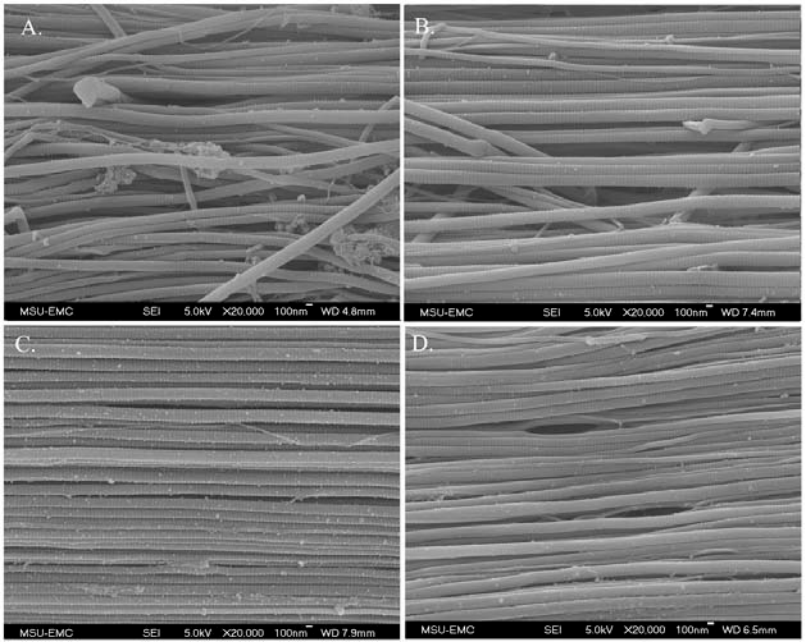

Figure 12 SEM images of control sample (A.), 0.1%/s (B.), 10%/s (C.), and 70%/s (D.) tests.

Statistical Analysis

The data in this study were presented as mean ± standard deviation (S.D.). One Way Analysis of Variances (ANOVA) was used for statistical analysis. The differences in D-period elongations were considered to be statistically significant when p is less than 0.05. Holm-Sidak test was used for post hoc pair-wise comparisons and comparisons versus the control group (SigmaStat 3.0, SPSS Inc., Chicago, IL). Tangent modulus values were found to be significantly different using post hoc pair-wise comparisons vs. the quasistatic rate when p is less than 0.05.

Results

The stress-strain curves showed strain rate sensitivity of tendon fascicles (Fig. 13).

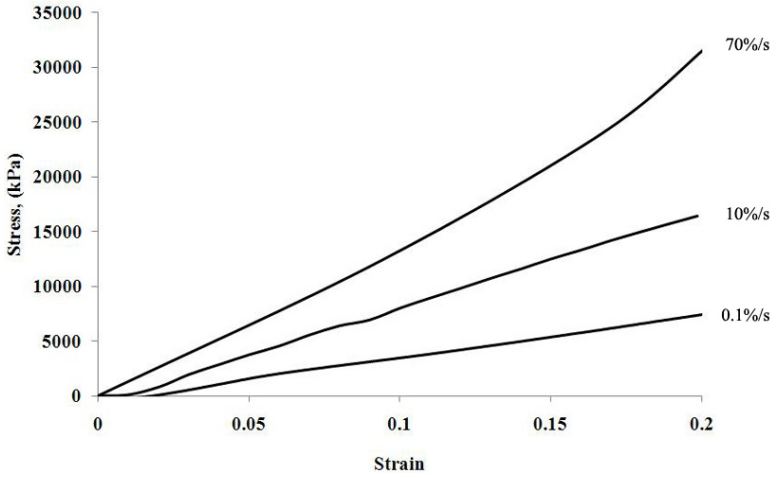

Figure 13 Tensile testing to 20% clamp-to-clamp strain with 3 different rates showing rate sensitivity (engineering stress vs. engineering strain).

Strain rate sensitivity was verified by an increasing tangent modulus with a strain rate increase. The tangent moduli in the linear region were found to have values of 102 ± 42, 195 ± 58, and 251 ± 116 MPa for 0.1%/s, 10%/s, and 70 %/s, respectively (Fig. 14).

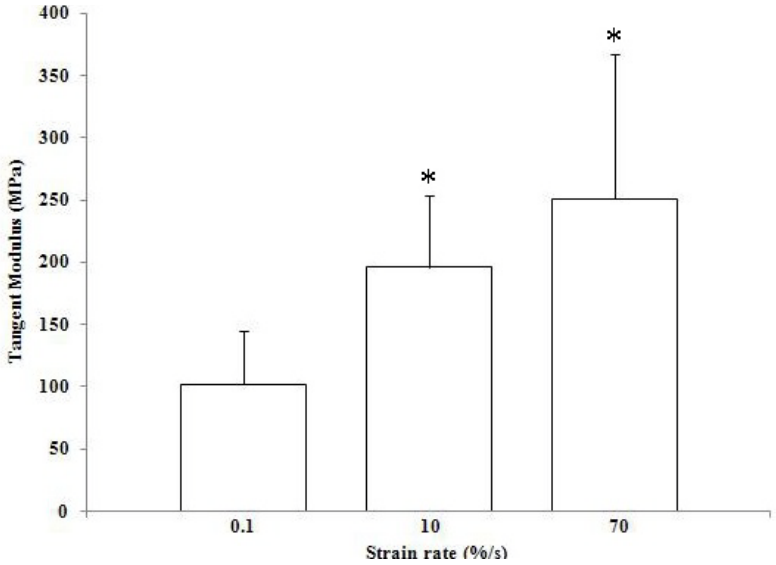

Figure 14 Average tangent modulus of tendon fascicles (n = 6), taken from 5% strain. *Indicates $p < 0.05$ vs. 0.1%/s.

Tangent modulus values were found to be significantly different using post hoc pair-wise comparisons vs. the quasistatic rate ($p < 0.05$). There was no difference found between 10%/s and 70%/s strain rates ($p = 0.32$) although there was an increasing trend.

The fixed fascicles were found to maintain their elongation after the removal of the tendon from the grips. SEM images showed a straightening of fibrils in strained fascicles compared to the less orderly control samples (Fig. 12). Elongation of the D-period was found to increase with strain rate increase (Fig. 15).

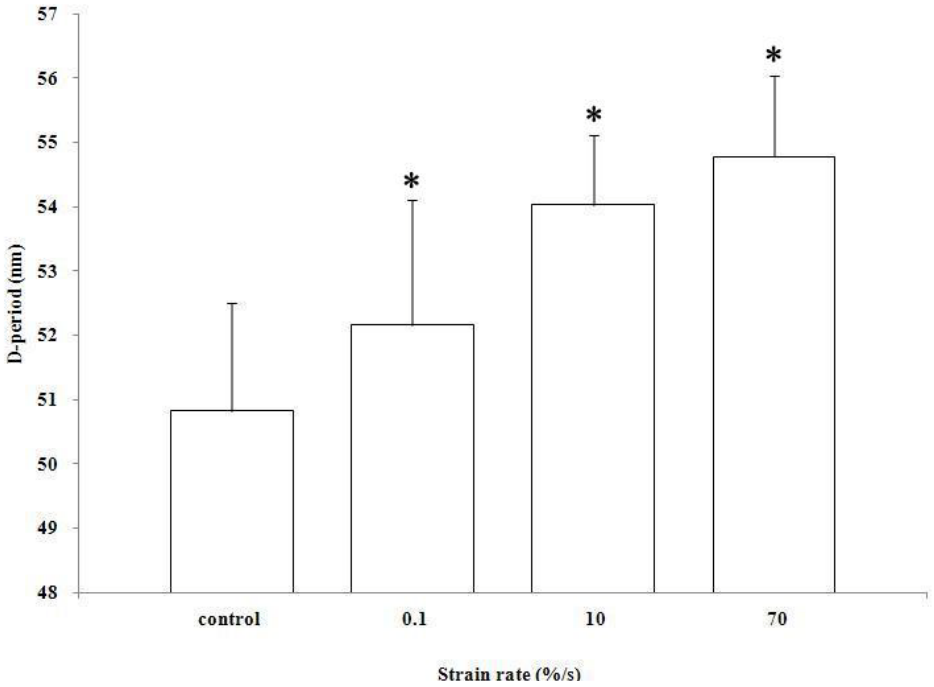

Figure 15 D-period analysis of 3 strain rates (n = 90) with measurements normalized to control (n = 50). *Indicates significant difference between all groups ($p < 0.005$).

For the control, 0.1 %/s, 10 %/s, and 70 %/s fascicles, the average D-period lengths were found to be 51.3 ± 1.4 nm, 52.2 ± 1.9 nm, 54.1 ± 1.0 nm, and 54.9 ± 1.2 nm, respectively. Statistical analysis found that all strain rates to be statistically significant from the control ($p < 0.005$). Each rate was also compared with each other and also was found to be significant ($p < 0.001$).

As expected, the analysis of the local midsubstance strain revealed a non-homogeneous strain field from clamp-to-clamp. However, our analysis showed that midsubstance strains for all 3 tests were around 12% in each strain rate group (10-14% local strain). Differences in local midsubstance strains were found to be insignificant

among different strain rate groups. Mechanical data revealed fascicles were not pulled past the linear region and proved no subfailure damage.

Discussion

In this study, patellar tendon fascicles were pulled to the same 12% local midsubstance strain level at different ramping speeds. The D-period was found to exhibit an increasing elongation as the rate increased. The results provide quantitative evidence, from the perspective of collagen fibril recruiting, that the tissue level mechanical response is ultimately dependent on the behavior at the lower length scales. Our data proves Puxkandl et al. and his speculation of an increasing fibril strain to tissue strain ratio relative to strain rate [73]. To our knowledge, this study is this first to reveal statistically significant data of increasing fibril elongation relative to the applied strain rate.

PGs have been known to participate in load transferring/bearing among a collagen fibril network [40, 73]. Screen et al. suggests the extracellular matrix is stiffer at higher strain rates due to its affinity for water [35]. Elliott et al. proved a larger and faster relaxation in matrix deficient fascicles [38]. Based on the dissipative theory [77], at relatively slow rates, the water and proteoglycan matrix have time to disperse and distribute forces, respectively. We speculate that at higher strain rates, fluid has less time to dissipate through the extracellular matrix and there is less time to distribute forces from collagen fibril to noncollagenous components [37, 81].

For the control, 0.1 %/s, 10 %/s, and 70 %/s fascicles, the average D-period elongation was 1.84 ± 3.6%, 5.5 ± 1.9%, and 7.03 ± 2.2% for the 0.1%/s, 10%/s, and

70%/s strain rates, respectively. Previous collagen fibril studies have used X-ray diffraction to monitor fibril strain during elongation of various tissue types. These studies are compared with the current patellar tendon study in Table 1.

Table 1 Comparison of the ratio of fibril strain to tissue strain (ϵ_F / ϵ_T). Collagenous tissues were from different animal models using X-ray diffraction for the D-period measurement. Tissue samples were loaded with similar quasistatic rates.

Primary Author, Year	Animal Model	Quasistatic Rate, %/s	Fibril Strain, ϵ_F	Tissue Strain, ϵ_T	Fibular Ratio Strain (ϵ_F/ϵ_T)
Current Study	Rabbit patellar	0.1	1.8	12	15%
Liao and Yang (2007)	Porcine mitral valve	0.6	0.5	12	4%
Liao et al. (2005)	Bovine pericardium	1	3.2	30	11%
Puxhandl et al. (2002)	Rat tail	0.08	3.3	9.5	34%
Mosler et al. (1985)	Rat tail	0.1	1.8	5	36%
Gupta et al. (2004)	Mineralized Tendon	0.1	3.37	7.46	45%
Krauss et al. (2009)	Deer Antler	0.005	1.23	2.46	50%
Gupta et al. (2005)	Bovine Femur	N/A	0.44	0.69	64%

Note: All data compared were analyzed from graphs in X-ray diffraction studies.

In this study, the quasistatic rate yielded a 1.84% strain in the fibril, correlating a 15% fibril strain to tissue strain ratio (ϵ_F / ϵ_T). The ratio of fibril strain to tissue strain is a definitive way of looking at mechanical function of the tissue. Heart valve showed low fibril strain to tissue strain, which possibly related to its mechanics and design to resist creep in constant cyclic loading [73]. Although there are no direct comparisons to the patellar tendon model, our study falls in between heart valve [73] and tissues less likely to undergo regular occurring tensile strain like antler [82] and bone [83]. There are differences in sample preparation and testing methods between the present SEM study and the X-ray diffraction studies in Table 1. We believe the difference in ϵ_F / ϵ_T is mostly attributed to biological variability and the compositional variation within those collagenous tissues.

The fascicle mechanical properties we reported in this paper were indirectly similar with previous studies. Yamamoto et al. reported a tangent modulus for 0.3 mm^2 rabbit patellar fascicles to be 180 MPa for a strain rate of 0.1%/s, higher than the 102 MPa for the 1 mm^2 fascicles found in the current study [84]. Although not a direct comparison, smaller cross-sectional area fascicles have been shown to have a higher modulus [81]. Human patellar tendon allografts (~50 mm^2) have shown a 239-306 MPa modulus at 100%/s [60, 85]. The current study calculated a value of 251 MPa for a 70%/s strain rate.

It is notable that the unstressed D-period reported in this paper was 51 nm, which is smaller than the typical 64-67 nm quantified in research [25-27] but comparable to D-periods measured by SEM and TEM technologies (53-54 nm) [28-30]. A shrinking of collagen fibrils regular occurs due to the chemical fixation and processing required for electron microscopy [31, 32]. We assumed the degree of collagen shrinkage due to chemical fixation and SEM processing was consistent throughout the sample and the change in the D-period length was disregarded as variability in the experiment.

The present study used ambient conditions as opposed to submerging samples in PBS. When taking fascicles out of their original conformation in the tendon, they are subjected to matrix swelling due to lack of constrain and have a "weakened" tensile strength [86]. Screen et al. noticed increased slipping and reduced mechanical properties with PBS incubated fascicles; they credit this swelling to GAG chains' ability to attract water [35]. We noticed that testing submerged fascicles resulted in prominent slipping between fibrils and a failed test with decreased tensile strength (data not shown;) we thus avoided a total PBS submersible experimental setting.

Fascicle mechanics in this study were more linear, less stiff, and more extensible than bulk tendon while also having a reduced toe region as seen in Figure 13 [38, 81]. Previous studies report a wide fascicle failure strain range from 8% to 21% [20, 21, 79, 84, 87, 88]. This wide range is most likely due to species/biological variability and experimental setup. Failure strains of fascicles in the present study were found to be approximately 15-20% local strain (data not shown). The local strain in the study (12%) was chosen to be close to ultimate stress and still within the linear region (to avoid aggressive subfailure damage). The current study did not investigate fibril failure. With the highest strain rate used in this study, the fibril underwent an average of 7% strain. Isolated collagen fibrils have shown to be linear from 4-7% strain [66, 89, 90]. We believe that fibril failure did not occur during our tensile testing. Substantial damage would have been evident with the presence of relaxed fibrils in the image analysis [57].

Our preconditioning protocol was adopted from Yamamoto et al. [20], subjecting fascicles to cyclic loading to a 2% strain and then a preload before tensile testing. Samples were preloaded with a 0.01 N load to remove slack from the fascicle while not approaching the toe region of the test. This usually resulted in an approximately 5-10 μm elongation. This additional elongation was taken into consideration in calculation of clamp-to-clamp strain.

Relaxation data was recorded after every test. Initial relaxation of tendon happens almost instantly after the ramping despite the fixative and to our knowledge is unpreventable. Although the samples underwent relaxation before fully cross-linked, the relaxation took place in a shorter period of time due to fast fixative infiltration and had more residual stress compared to fascicles submerged in hydrating buffer. Without

fixative, our fascicles showed a ~40% relaxation and reached equilibrium at 1300 seconds. Our data showed that, in the glutaraldehyde fixative, the stress in the fascicle relaxed approximately 15% and reached equilibrium at 200 – 300 seconds, showing the effect of glutaraldehyde and the speed of the cross linking. If faster fixatives could have been used or if an instant capture of the fibrils immediately after loading was feasible, we speculate that our results would have had slightly higher measurements in fibrils strains.

The number of animals in this study was small compared to our fibril sample number. We decided to follow the procedure of Kukreti et al. to exhaustively analyze D-period measurements throughout the midsubstance of three separate animals rather than analyzing fewer images and a greater number of animals [28]. Our SEM analysis averaged fibrils throughout the midsubstance and not in one localized area. This different method represents what is happening throughout the sample and accounts for errors likely caused by local variability [52, 88, 91].

Although grip slippage did not affect our conclusion, an improved clamping technique is still needed. There was no significant difference in modulus taken from the two highest rates, although there was still an increasing modulus trend. The reason we did not investigate higher strain rates in this study was due to the limitation of the mechanical testing device. The tensile testing machine in the current study proved to be accurate up to around 5000 μm/s corresponding to the study's highest rate (70%/s). With a relatively small sampling rate, the 70 % /s tests in Figure 13 had less of a toe region and a more linear increase of stress. Faster strain rates and sampling rates will be investigated in our future study. Future studies will also be focused on tendonitis and chronic collagen disorders and their affect on fibril kinematics.

In conclusion, our finding unfolds an underlying mechanism of tendon strain rate sensitivity. We conclude that collagen fibrils undergo a significantly greater degree of elongation, relative to the tissue strain, at higher strain rates. This mechanistic finding provides insight into the behavior of the tendon at the micro scale and establishes a basis for future development of constitutive models.

CHAPTER III

THE MECHANICAL RESPONSE OF TENDON UNDER HIGH RATE COMPRESSION WITH BRAIN AND LIVER COMPARISON

Introduction

Knowledge of the mechanical properties of human tissues under different loading conditions is needed for the development of accurate computational models. Quasistatic characterizations of soft tissue have been thoroughly studied; however, higher rate impacts of soft tissue have not been well investigated and cannot be described by extrapolating mechanical data from quasistatic tests. Thus, high rate mechanical testing must be performed to properly describe soft tissue responses.

We considered the polycarbonate split Hopkinson pressure bar (SHPB) apparatus to establish a sound high strain compression model. The SHPB has the ability to apply compressive stresses at 100–10,000 /s [92] and has been applied in metal mechanics. The SHPB system is based on the elastic wave propagation theory and the principle of superposition of waves: the stress, strain, and particle velocity can be estimated by analyzing the reflected and incident waves at any cross-section[93].

Recently in the SHPB model, polymeric bars have allowed testing of softer materials that have similar acoustical impedance of bars. Unlike metal bars, polymeric bars enable a smooth transfer of energy during the impact of the incident bar and tissue, resulting in less noise in the data acquisition [94]. The downside of polymeric bars is that

the waves experience attenuation, or a gradual weakening of transmission, and they gradually become warped over time of high rate testing. Testing these bars on soft tissues has brought up new concerns including a hardening effect that occurs at the beginning of compression tests, an effect that some choose to ignore and disregard as an inertial effect [92, 94].

The brain and liver are two of the most commonly injured organs. The ongoing efforts of the CAVS biologically inspired team include brain and liver high rate studies. During the studies, we noticed the high rate stress-strain curve of brain and liver both showed an initial peak, followed by softening and then hardening. We found that the initial peak of brain is higher than liver. Some previous studies on muscle tissue also showed similar trend, but no conclusion has been reached in terms of underlying structural mechanism of the initial peak.

After examining the composition and ultrastructure of brain and liver, we noticed that both water content and cellular content could potentially affect the high rate response. We hence hypothesize that the underlying mechanism of high rate response of soft tissue is related to how water and cells react to a fast relocation. To validate this hypothesis, a polycarbonate split Hopkinson pressure bar (PSHPB) was used to apply high rate compression of tendon, liver, and brain in both wet and dry states. Porcine liver and brain tissues were compared with porcine tendon to explain phenomenological effects of high rate loading on soft tissues. Brain, liver, and tendon have similar water content (80%, 70% and 70% respectively), but various cellular content. The PSHPB experiments of three types of tissue at either hydrated or dehydrated status provide important clues to determine structural mechanisms of tissue high rate response.

Histology and SEM imaging of all tissues in each condition were further examined to reveal the structural contribution and the effects of lyophilizing.

Previous High Rate Studies

There have been previous studies using the SHPB apparatus for soft tissue experimentation. Song et al. tested porcine muscle along two perpendicular directions at dynamic strain rates up to 3700 s^{-1} and found that both directions showed a nonlinear, strain rate dependent behavior [94]. They believed that the early spike (an initial hardening peak) found in high compression tests of soft tissues has not been determined as part of the material's intrinsic response and is more likely a radial inertia effect of the sample. The specimen used was a disc shaped specimen with the inner 30% of the sample cut out to minimize axial stress along the radial direction and in turn decreasing the inertial effect. This proved to minimize the initial spike of the compression test. Similarly, Van Sligtenhorst et al. found the mechanical response of bovine muscle at strain rates up to 2300 s^{-1} to be strain rate dependent and proved to emit an inertial response[92]. Sligtenhorst found an increase in compressive modulus with strain rate by analyzing the sample's stress at 30% strain. There was also a similarity in tissue behavior between fresh and aged samples. The Hopkinson Bar has also been applied to tendon in high rate tension. Cheng et al. investigated the effect of high rate repetitive, tensile loading of bovine tendon [95]. Samples undergoing fast and slow rates experienced a stress softening the first few cycles known as the Mullins effect (a sample loaded past the previous test in strain will follow the unloading path of that previous test.) Chen et al. compressed porcine liver up to 1550 /s and found an increase in stiffness and initial peak

values with increasing strain rate[96]. They also showed a directional insensitivity. Prabhu et al. showed an increase in stiffness and initial peak values with no differences in the response of the left and right hemispheres [97].

Justification

This study sheds light on mechanistic understanding of how soft tissues undergo high speed deformation and challenges previous studies, which have disregarded the initial peak during the compression test as an unrelated inertial effect that does not characterize the tissue's intrinsic properties. Experimental results of soft tissue under high strain rate conditions could potentially be incorporated to human models which in could optimize safety measures that could reduce the risk of human injuries and death in high-impact situations.

Methods

Sample Preparation

Porcine liver, brain, and tendon from healthy adult pigs were obtained from Sansing Meat Services in Maben, MS. The specimens were stored in PBS under ice soon after extraction and during transportation to the laboratory. All native tissue testing was performed within 12 hours of extraction. For SHPB testing, samples were carefully extracted to certain parameters. A cylindrical die of 30 mm inner diameter was used to cut brain and liver samples to approximately 27 mm in diameter and 9 mm thick for a consistent 3:1 aspect ratio. The diameter of tendon samples was cut using a 10 mm cylindrical die for the transverse directional testing, giving an approximate 9 mm

diameter. Axial direction compression of tendon involved manually adjusting the elliptical cross section using sharp dissection until the diameter closely resembled that of the circular, transversely loaded samples (axially loaded samples had an approximate 8 mm diameter). Stress was normalized to each samples' dimensions for each test.

Bulk samples subjected to freeze drying were dissected and immediately weighed for water percentage. They were then stored in a cylindrical 30 mm diameter container at -4˚C until the lyophilizing process. Frozen samples were lyophilized using a Freezone™ 1 liter bench top freeze dryer (LABCONCO®) for approximately 48 hours under 0.1 Pa and -50˚ C. Samples were then weighed to verify a 100% water loss. Due to sample shrinkage, bulk tissue was freeze dried then cut for testing. The lyophilized bulk tissue was then cut into discs, 9 mm thick with an approximate 27 diameter, giving the lyophilized tissue the same dimensions as the native samples. The dried samples were then tested under the same SHPB conditions as the native tissue testing.

Image Analysis

Native tissues underwent qualitative analysis with wet SEM imaging using a Zeiss Evo® 50 scope to look at structure properties of the tissue in their hydrated state. Samples were obtained from 15-20 kV all at 300X magnification. The Evo scope was operated in the water vapor mode, not allowing the samples to readily dry out. Native tissue samples were also subjected to rhodamine phalloidin and DAPI staining; samples were fixed in 10% neutral buffered formalin and dehydrated in a graded ETOH series. The samples were then embedded in Paraplast with CitriSolve as a transitional fluid, sectioned to a thickness of 7 μm, and stained with rhodamine phalloidin. In staining,

DAPI labeled cell nuclei blue and rhodamine labeled the actin filaments of the cellular cytoskeleton red.

The microstructure of lyophilized samples was viewed using a JEOL JSM-6500 FE Scanning Electron Microscope. Lyophilized samples were cut using sharp dissection to reveal their cross-section of the sagittal plane. Samples were then mounted on aluminum stubs and sputter coated with gold-palladium before SEM viewing.

Image Analyzer v.2.2-0 software (CAVS, Mississippi State University) was used for analyzing SEM images of the lyophilized tissues for cavities that resemble both cellular voids and structural composition. The parameters obtained for each image during analysis included object count, area fraction, mean area of object, and mean nearest neighbor distance (nnd). Area fraction is the ratio of the total cavity body area to total image area. Mean area of object represents the average area of all cavities found in the image. Mean nnd is a measure of the average distance between neighboring cavities. Analysis was limited to areas around ~5μm^2 or larger. There were three animals representing the three images analyzed for each tissue (brain, liver, and tendon.)

SHPB Testing

The PSHPB setup includes 38.1 mm diameter polycarbonate (PC 1000) rods and composed of a striker bar, an incident bar, and a transmitted bar with lengths 0.76, 2.44, and 1.22 m, respectively (Fig. 16).

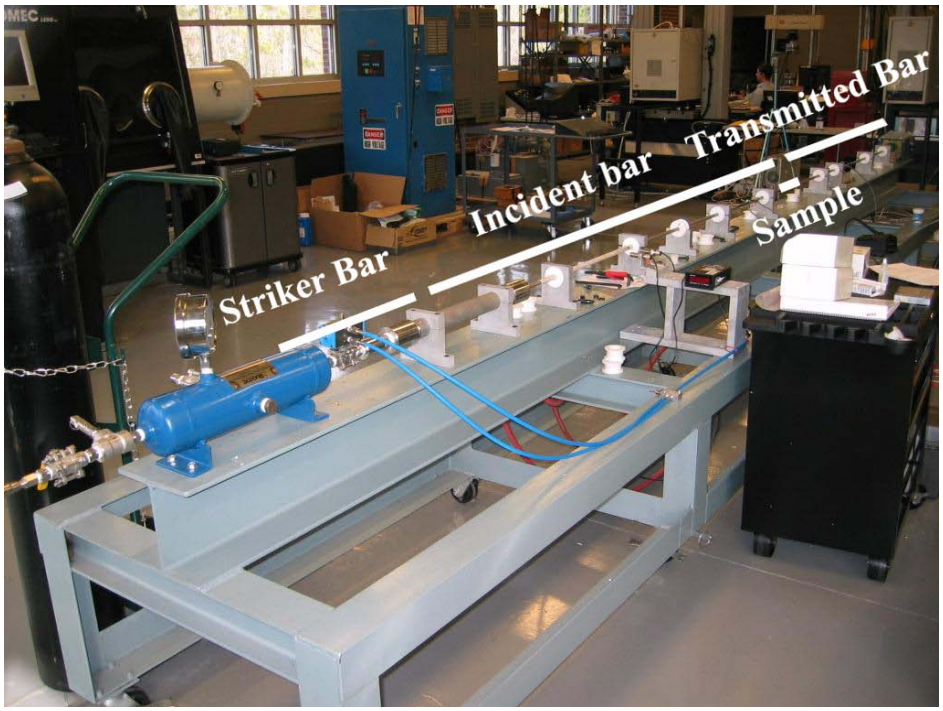

Figure 16 The SHPB system with bars and sample placement labeled (Courtesy of CAVS, cavs.msstate.edu.)

Strain gauges are attached to both the incident bar and transmitted bar. Details involving sample placement and wave theory were adapted from previous studies[96, 97]. Briefly, for every test the sample was glued using cyanoacrylate glue between the incident and transmitted bars (Cemedine, Japan) [98, 99]. Native tissues were kept hydrated with PBS throughout testing procedures. A manual switch activates the pneumatic pressure system and forces the striker bar at a specified pressure into the incident bar. The initial impact sends waves through the incident bar and then through the sample causing compression and on through the transmitted bar. There is an incident wave (the wave propagated through the incident bar), reflected wave (reflected from the sample to the incident bar), and a transmitted wave (the wave that remains after propagation through the sample

measured by the transmitted bar strain gauges.) The setup also includes a velocity laser gauge and DAQ modules that acquired the strains of the incident and transmitted bars.

Three different porcine tissues' mechanical data were compared. Dry and wet brain data sets were done by Michael McCollum and Rajkumar Prabhu [97]. Initial hardening effects caused by high rate loading of native tissues were also compared to lyophilized samples of the same origin. A strain rate of 550 /s was used for all of the comparison high rate tests while a 750 /s strain rate was also used for tendon samples. There were three samples of each tissue used for each test group (n = 3) except for brain (n = 5). Maximum stress and the initial hardening peak values were computed for all samples tested. The elastic modulus was also used in comparing tendon's mechanical properties and taken from the corresponding stress at 30% strain [92]. This strain was at the beginning of the linear region for the tendon tests.

Statistical Analysis

The data in this study were presented as mean ± standard deviation (S.D.). One Way Analysis of Variances (ANOVA) was used for statistical analysis. The differences in elastic modulus of tendon samples between strain rates as well as loading directions were both considered to be statistically significant when p is less than 0.05 (SigmaStat 3.0, SPSS Inc., Chicago, IL). Initial hardening peak values were also found to be significantly different when p is less than 0.05. Ultimate stresses reach between the wet and dry samples were significantly difference when p is less than 0.01 for the tendon group and p less than 0.001 for the liver group. Wet and dry brain tests did not reach

significantly different maximum stresses. Sample numbers were all n = 3 except for brain tests (wet and dry), which was n = 5.

Results

Three porcine tissues, in hydrated and dry states, were successfully compared at high rate. Native tissues in their hydrated state were viewed under wet SEM and subjected to qualitative analysis to examine native, structural differences amongst the three tissue types (Fig. 17). Hydrated tissues were also subjected histology to view cellular and nuclear distribution and morphology (Fig. 18).

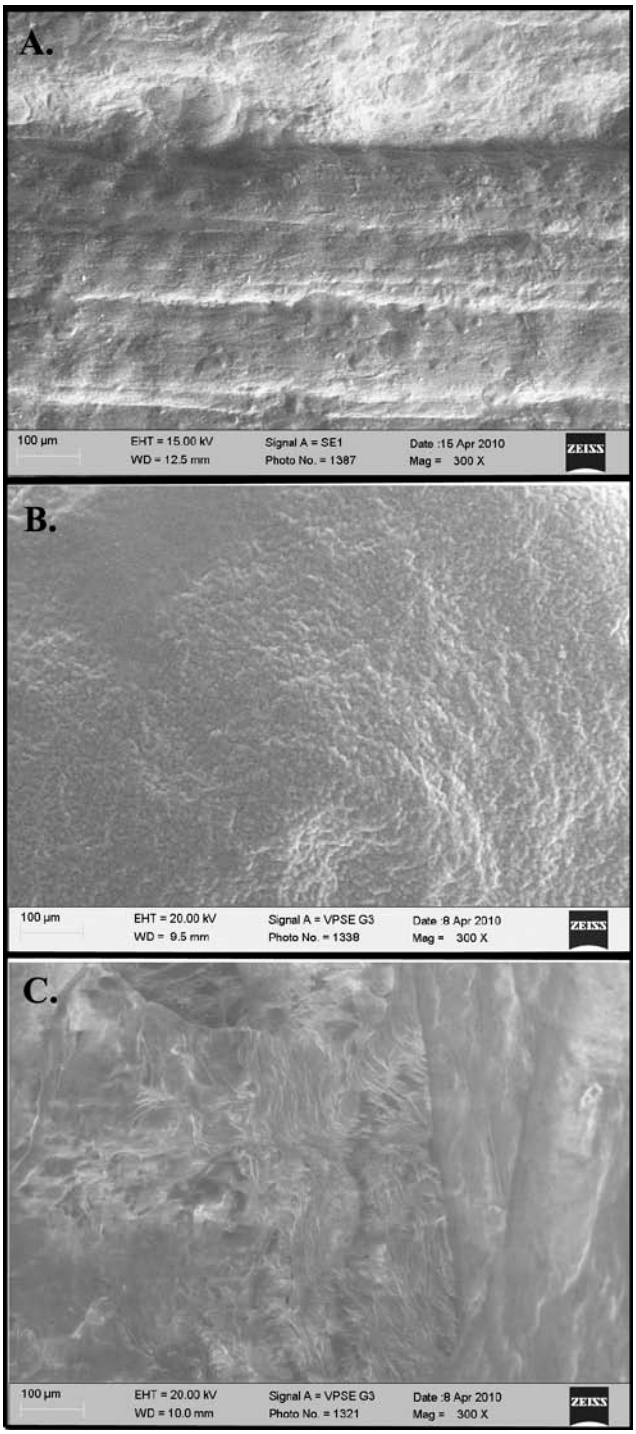

Figure 17 Evo SEM images of all three hydrated tissues: tendon (A.), liver (B.) and brain (C.). All images are at 300X.

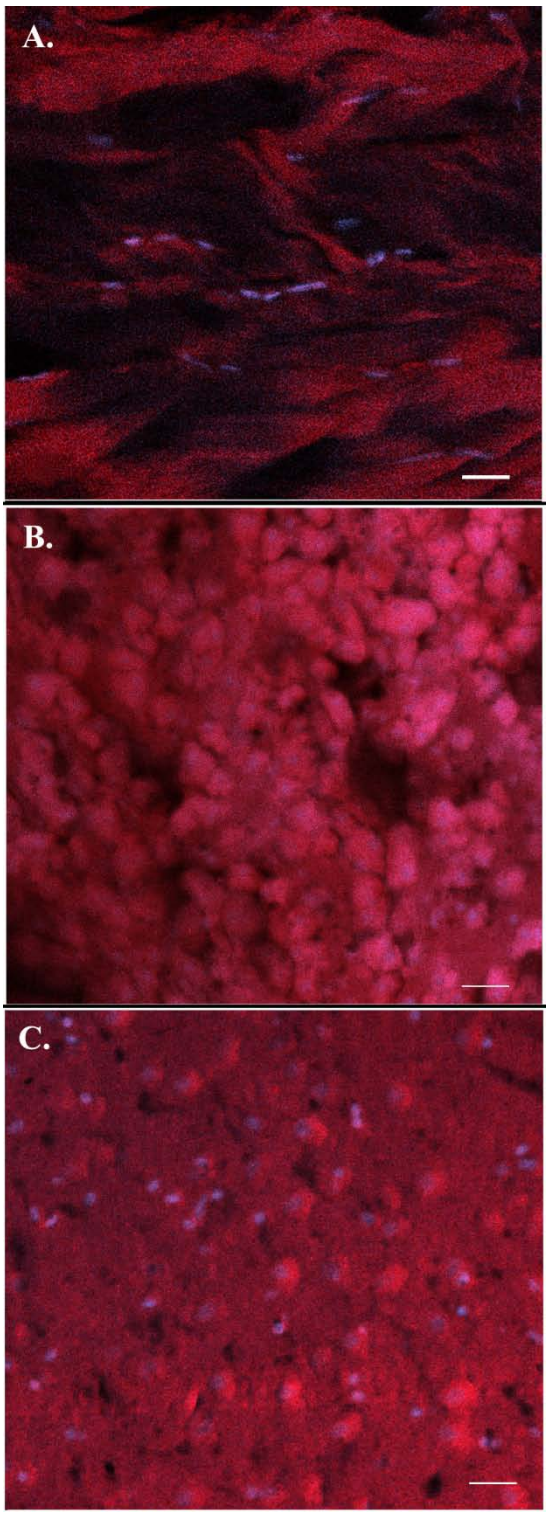

Figure 18 Histology of all three hydrated tissues: Tendon (A.), Liver (B.) and Brain (C.) All images are at same magnification (Scale bar = 20 μm).

Image analysis was not done on histology images. Histological staining revealed cellular morphology of all three tissue types. Although having similar water percentage as the other two tissues, tendon contains very few cells, which have slim and elongated shapes.

Image analysis of lyophilized tissues subjected to SEM revealed significant trends. Using the cross section, the area fraction of voids was the smallest in tendon and the largest in brain with a significance of $p < 0.05$. All images were taken at the same magnification. Tendon was viewed axially due to no structural voids or gaps along its transverse axis (Fig. 19). Liver (Fig.20) and brain tissue (Fig. 21) were viewed from their sagittal planes. Dry tendon, liver, and brain were calculated to have an average of 0.03 ± 0.02, 0.3 ± 0.07, and 0.49 ± 0.26 area fractions, respectively (Table 2).

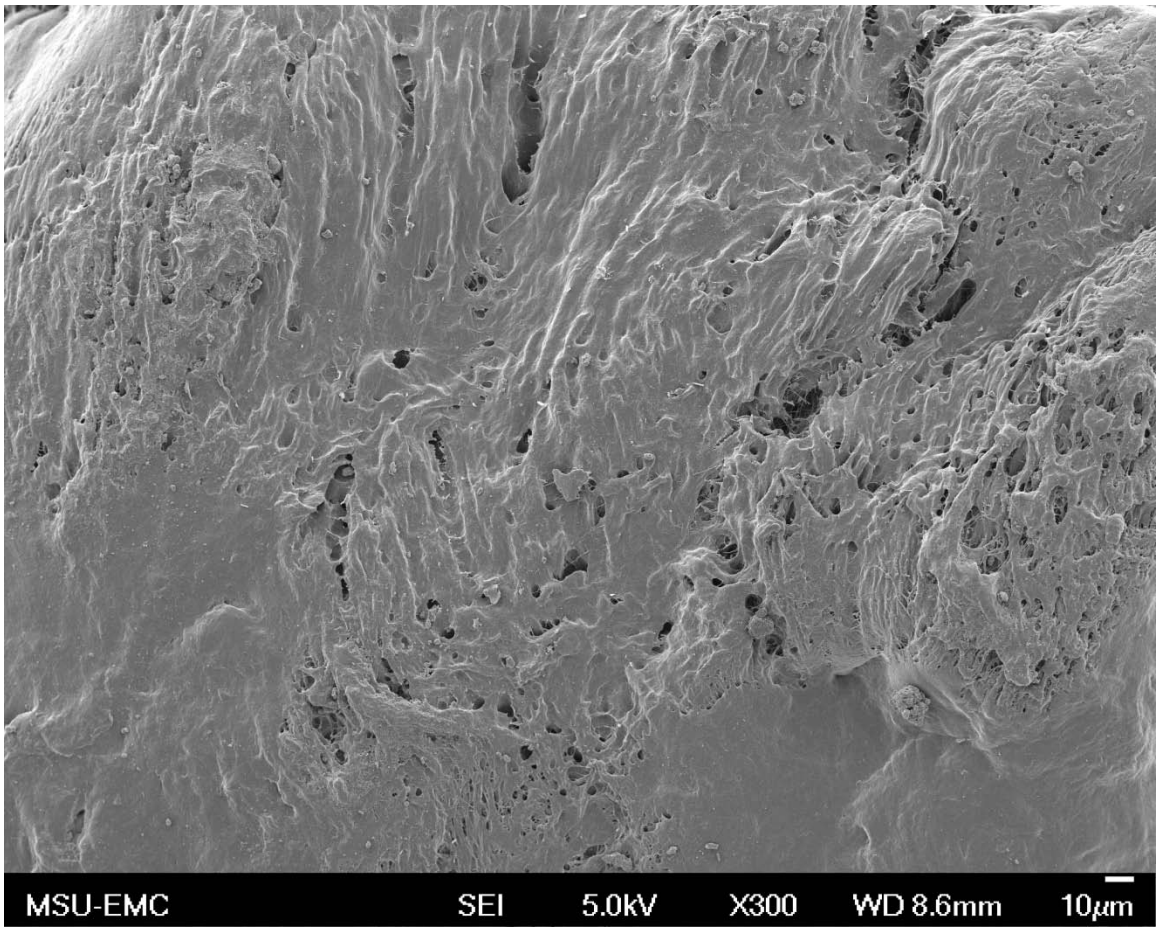

Figure 19 SEM image of lyophilized tendon along its longitudinal axis.

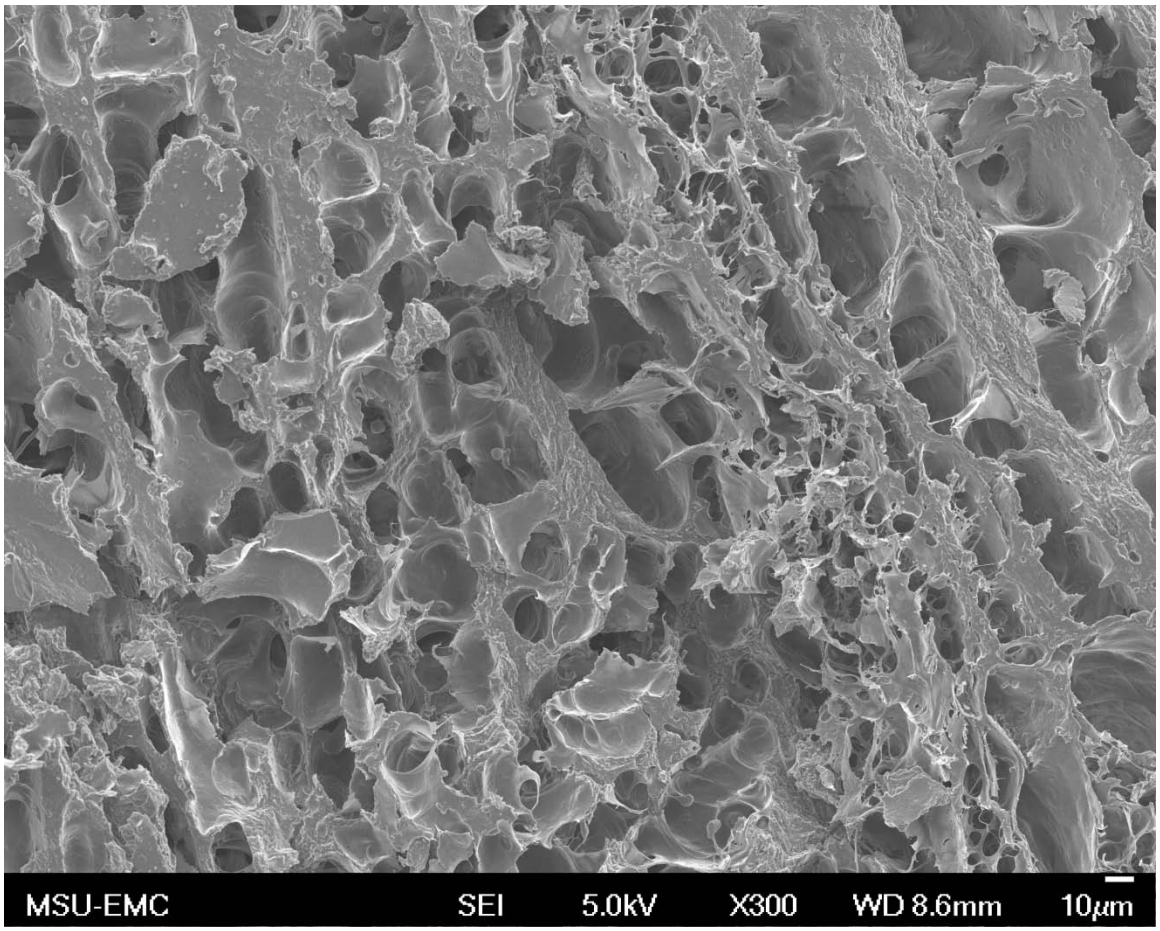

Figure 20 SEM image of lyophilized liver.

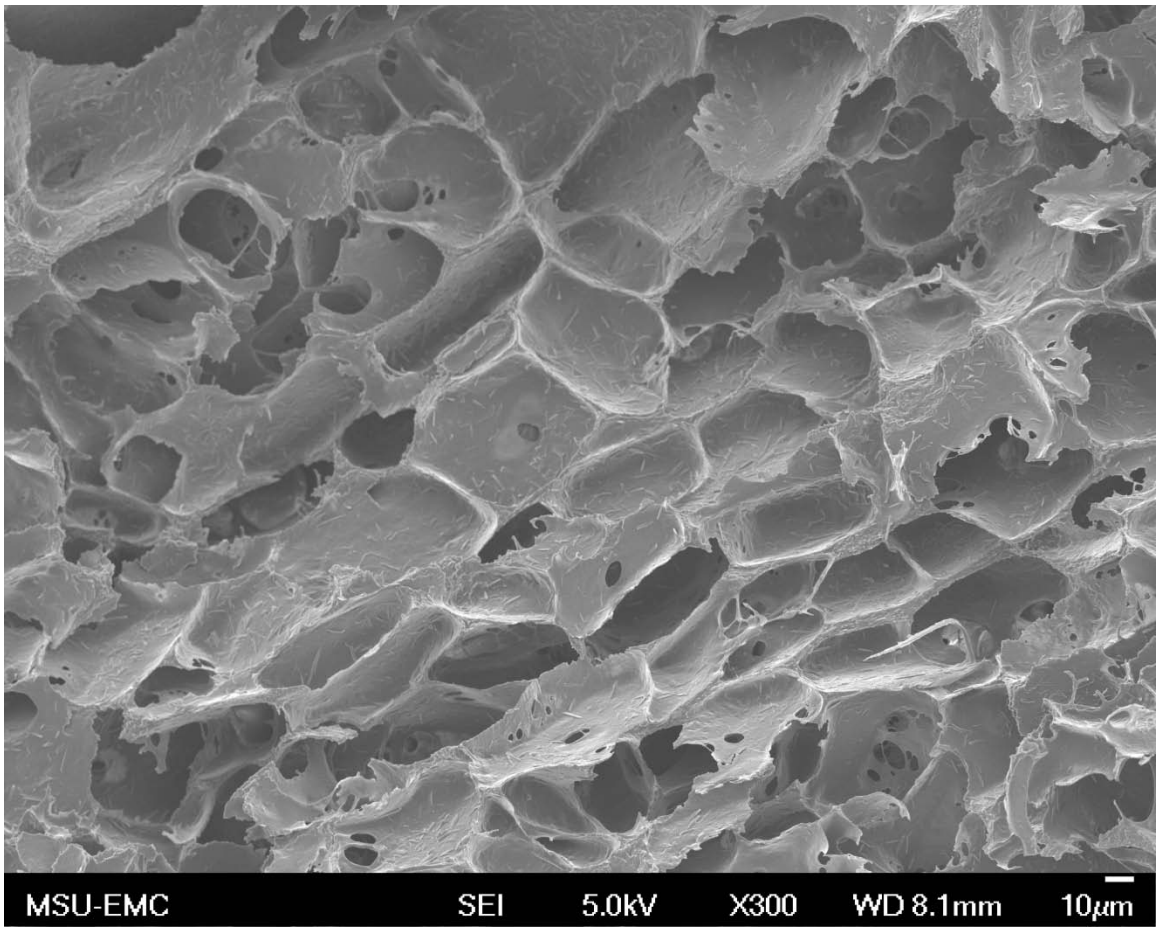

Figure 21 SEM image of a completely dried brain sample, which had the largest cavities among the tissues.

Table 2 Image analysis of SEM images of dried tissues.

Tissue	Object Count	Area Fraction	Mean Object Area (μm^2)	Mean NND (μm)
Dry Tendon	20 ± 8	0.03 ± 0.02*	7 ± 4	12.4 ± 11.9
Dry Liver	1427 ± 384	0.3 ± 0.07*	104 ± 77	9.8 ± 4.0
Dry Brain	638 ± 55	0.49 ± 0.26*	242 ± 150	11.4 ± 8.2

*p-value < 0.05

Porcine tendon, liver, and brain tissues were successfully compared under high rate in both native and completely dry states. There was also a notable difference in the

initial hardening effect among all three samples (Fig. 22). The mean initial peak values had a significant difference ($p < 0.05$), tendon having the lowest (0.02 ± 0.01 MPa) and brain having the highest (0.22 ± 0.12) (Fig. 23). As expected, lyophilized samples all reached higher ultimate stresses than the corresponding native tissue (Table 3). There was no evidence of an initial hardening peak in the dried samples of brain (Fig. 24), liver (Fig. 25), and tendon (Fig. 26).

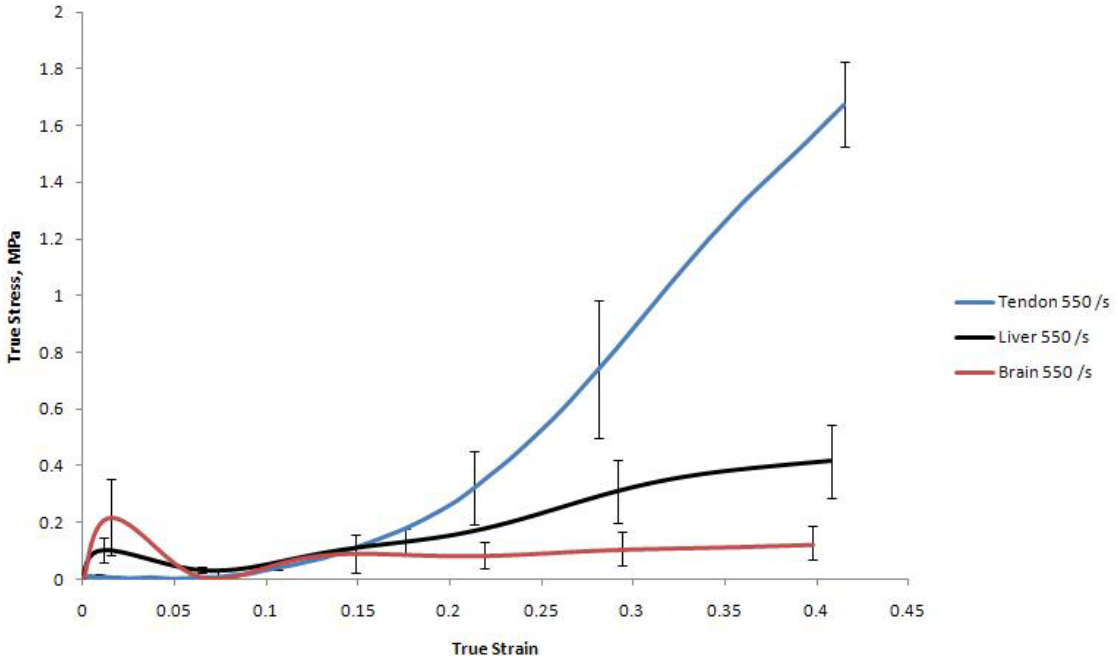

Figure 22 High rate compression of three different porcine tissues at same strain rate, 550 /s (n = 3 for tendon and liver; n= 5 for brain).

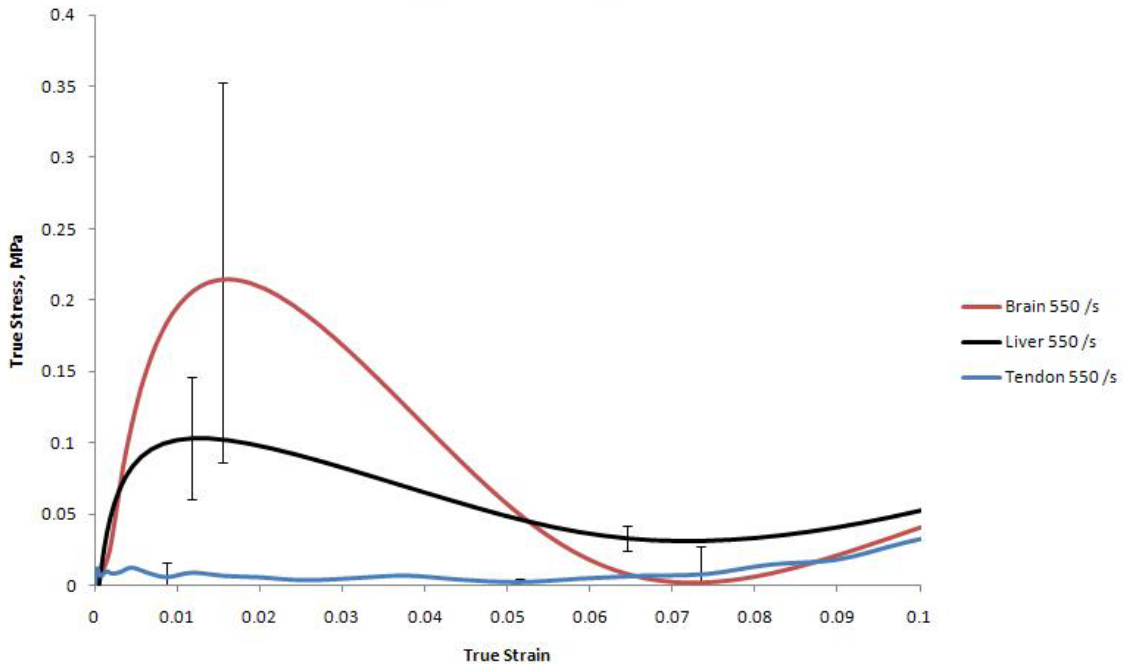

Figure 23 The initial hardening effect occurring at the initial impact of high rate testing (n = 3 for tendon and liver; n= 5 for brain).

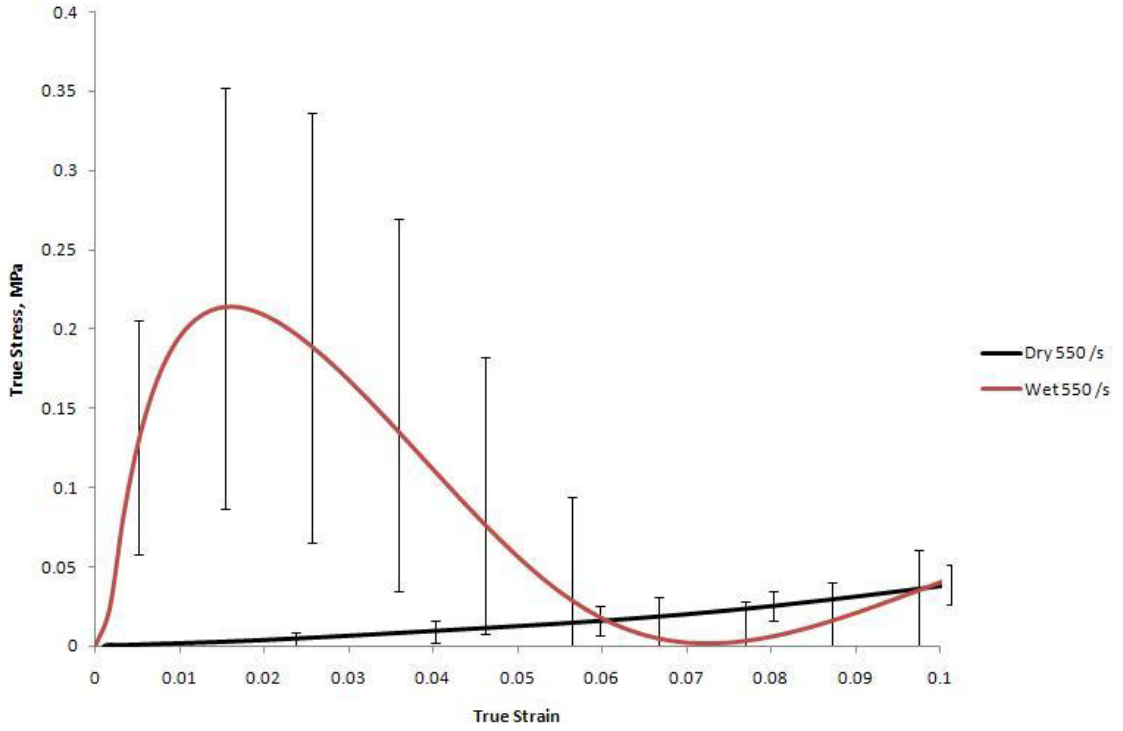

Figure 24 Dry and wet brain compression testing (n = 5).

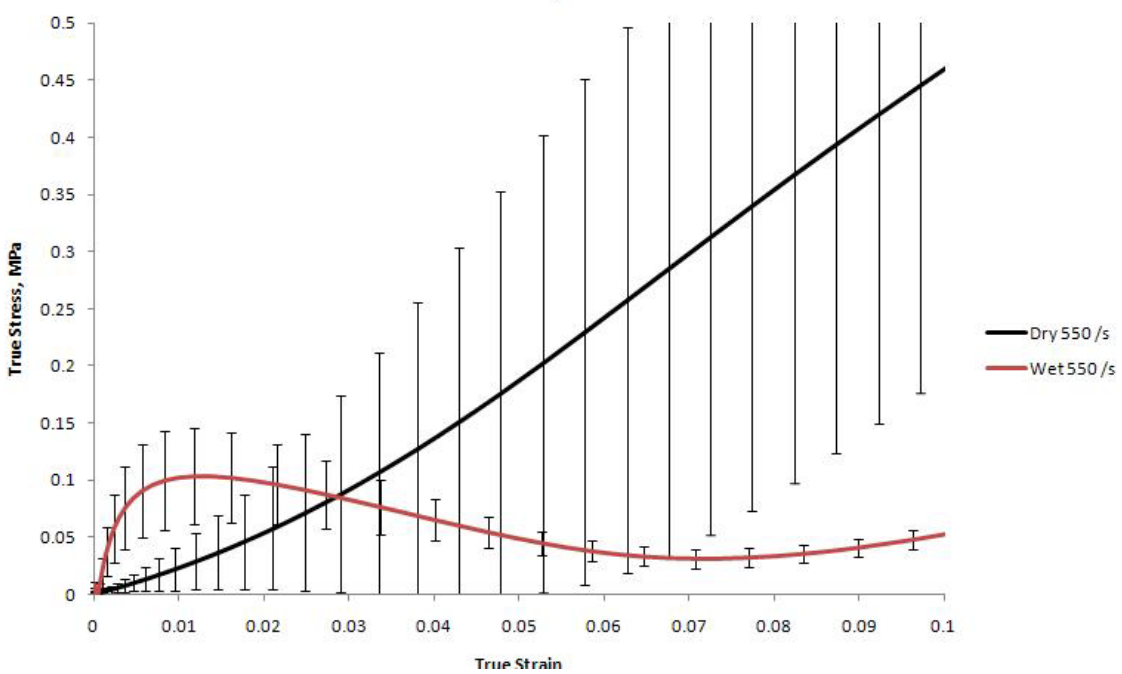

Figure 25 Dry and wet liver compression testing (n = 3).

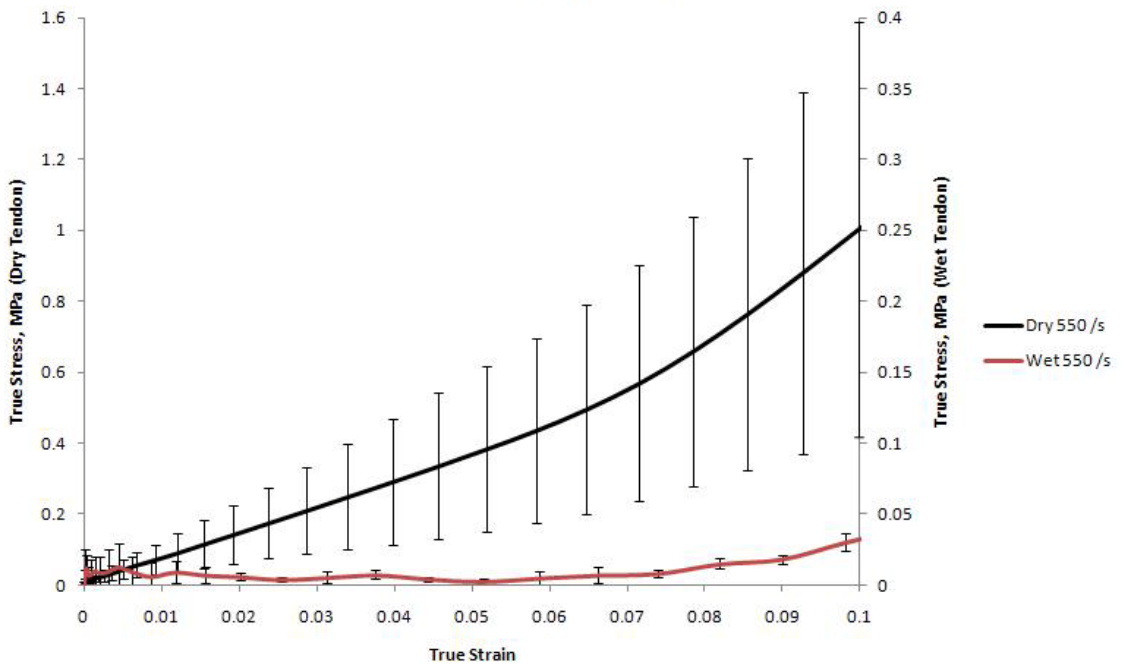

Figure 26 Dry and wet tendon compression testing (n = 3). Axis on right intended for only wet sample (lower curve.)

Table 3 A comparison table of all three tissues in both wet and dry states at 550 /s in compression.

Tissue	State	Initial Peak (MPa)	Ultimate Stress (MPa)
Tendon	Wet	0.02 ± 0.01*	4.05 ± 0.29#
Tendon	Dry	-	9.84 ± 1.72#
Liver	Wet	0.1 ± 0.04*	0.44 ± 0.13♦
Liver	Dry	-	1.76 ± 0.19♦
Brain	Wet	0.22 ± 0.12*	0.12 ± 0.07
Brain	Dry	-	0.13 ± 0.10

*$p < 0.05$ ♦$p < 0.001$
#$p < 0.01$

Tendon was subject to high rate compression testing to characterize mechanical properties under high rate conditions. As expected, strain rate sensitivity between 550 /s and 750 /s rates (Fig.27) and directional sensitivity between transversal and axial loading directions (Fig.28) were seen in the mechanical curves of the native samples. Strain rate sensitivity had a significance of $p < 0.05$ and directional dependence also had a significance of $p < 0.05$ (Table 4). As expected, the strain rate ($p < 0.01$) and loading direction ($p < 0.001$) affected the maximum stress reached by the wet tendon samples.

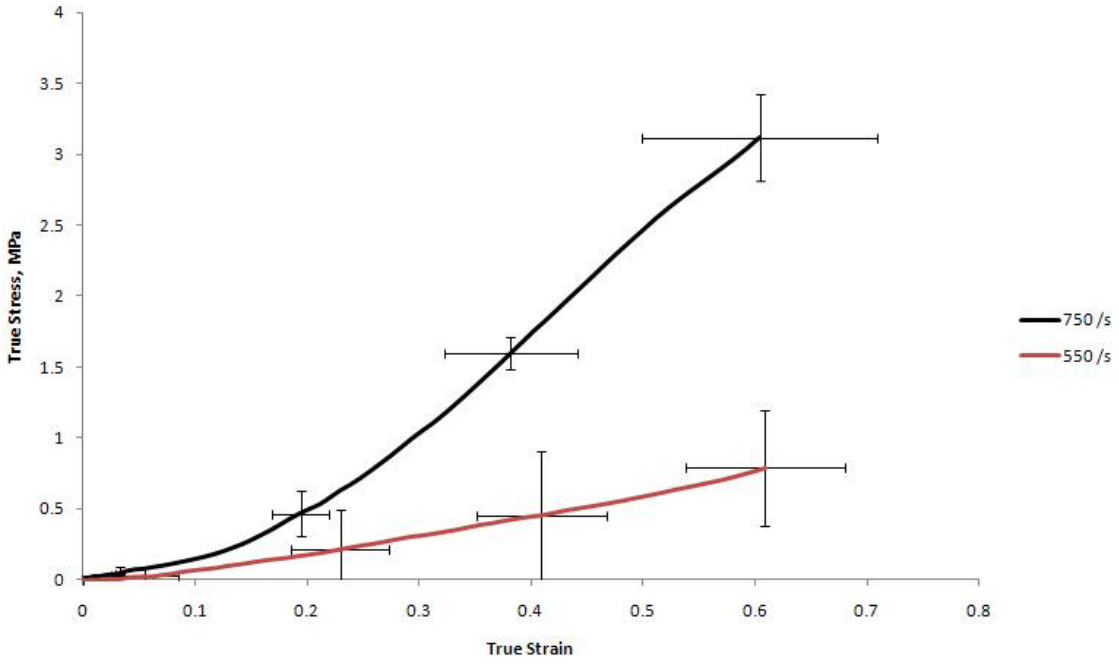

Figure 27 Native tendon compressed at different strain rates in the same axial direction (n = 3).

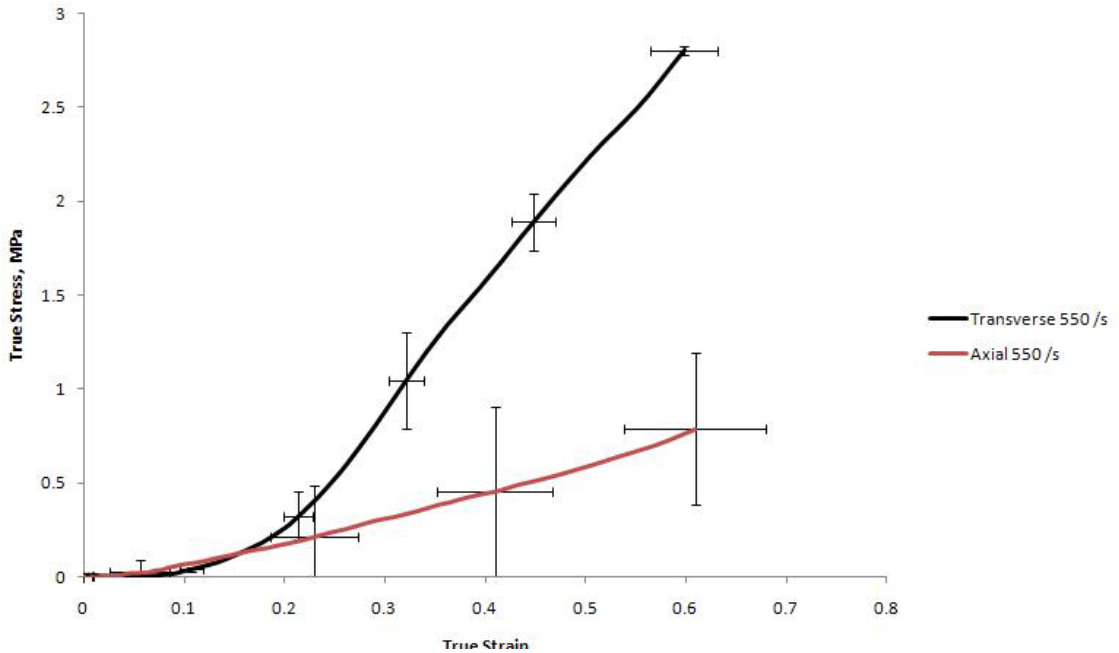

Figure 28 Native tendon compressed at different loading directions at the same strain rate, 550 /s (n = 3).

Table 4 Tendon's mechanical characteristics under high compressive loads showing directional and strain rate sensitivity. Modulus was taken at 30% strain.

State	Direction	Rate (/s)	Modulus (MPa)	Ultimate Stress (MPa)
Wet	Axial	550	$0.91 \pm 0.89^{*\dagger}$	$1.22 \pm 0.37^{=\blacklozenge}$
Wet	Axial	750	$3.53 \pm 1.00^{*}$	$4.01 \pm 0.63^{=}$
Wet	Transverse	550	$3.13 \pm 0.58^{\dagger}$	$4.05 \pm 0.29^{\blacklozenge}$
Dry	Transverse	550	14.47 ± 4.20	9.84 ± 1.72

$^{*}p < 0.05$ $^{=}p < 0.01$
$^{\dagger}p < 0.05$ $^{\blacklozenge}p < 0.001$

Discussion

To further examine the relationship between the tissue type and its material response, analysis of mechanical behavior was performed by analyzing the ultimate stress and the initial peak (Table 3). The ultimate stress was higher in both dry liver and dry tendon than the corresponding native samples. No difference was found in the ultimate stress reached by both dry and wet states of brain tissue most likely due to the lack of structural contribution after the lyophilizing process. SEM images of dried brain showed mostly cellular spacing and thin walls of tissue surrounding the cavities. All three tissues have similar water content: 65%, 70%, and 78% for tendon, liver, and brain, respectively. Tendon showed a minimal early spike in the test and was similar in water content compared with the other tissues but had a large difference in cell count (validated by histology) and cellular space (validated by SEM). At high rate impacts, soft tissues with higher cellular space (not just high water percentage) rely more on a viscous nature with first contact. The first contact could send an initial wave that collapses cellular spaces as it propagates.

Prabhu et al. [97] and Chen et al. [96] revealed an increase of these initial peak values with increased strain rate with the compression of brain and liver, respectively. Initial hardening stress values between tendon, liver and brain had a significant difference ($p < 0.05$), tendon having the lowest (0.02 ± 0.01 MPa) and brain having the highest (0.22 ± 0.12). As expected, due to the elimination of water content, lyophilized samples all reached higher stresses than the corresponding native tissues and had no evidence of an initial hardening peak. This leads to a speculation of more than just an inertial effect and an accurate representation of a tissue response dependent on both water content and cellular space (shown by lyophilizing and tissue type, respectively). The inertial effect should not be disregarded as a reaction unrelated to the tissues intrinsic response as more research is clearly needed.

Tendon was found to be rate dependent between the rates of 550 and 750 /s with a significance of $p < 0.05$ (Table 4). As expected, the higher strain rate was also found to have a larger ultimate stress. Tendon was also found to be directionally dependent ($p < 0.05$), having a difference in the axial and transverse loading directions.

Lyophilized tissues were subject to image analysis based on their voids or cavities. These cavities were most likely cellular space and can be speculated that the area fraction of dry tissue voids can represent cellular content. The SEM images were taken of the tissues cross-section of the sagittal plane. The cross-section was prepared by sharp dissection of the lyophilized sample and could possibly have caused microscopic artifacts in the images and caused an error in the image analysis. Ideally, a histological analysis of the tissues cellular area fraction would be best suited for this study.

Tendon characterization was done by taking the elastic modulus of the curve around 30% strain (Table 4). This was done because this strain was corresponded to the beginning of the linear region of the mechanical curves [92]. Tendon samples were 9 mm in diameter in axial loading tests and 10 mm in diameter in transverse testing. Although this is significantly smaller in diameter compared with the brain and liver samples, the SHPB assumes a one dimensional compression during the test. The SHPB system is based on the principle of superposition of waves where stresses can be estimated by analyzing the reflected and incident waves at any cross-section [93].

In conclusion, tendon characterization at high rate compression was successfully achieved and the tissue was deemed both strain rate and directional dependent. High rate testing on three different porcine tissues successfully revealed trends based on water content and area fraction (lyophilized cavities implying cellular space). More research is warranted before the inertial effect is to be disregarded and assumed unrelated to the tissue's intrinsic response. Future studies will include an in-depth histology analysis, relating other tissues with difference in water content, and varying lyophilizing in the tissue to see a gradual effect of water loss. Tissues like articular cartilage (having 80% water and the one of the lowest density of cells of any body tissue) should also be tested to strengthen the theory of cellular space and content affecting the tissue response. Experimental results and computational simulations of liver and brain tissue under high strain rate conditions could be incorporated into a human model which could reduce the risk of human injuries and death in high-impact situations.

REFERENCES

1. Butler, D.L., et al., *Biomechanics of ligaments and tendons.* Exerc Sport Sci Rev, 1978. 6: p. 125-81.

2. Wang, J.H., *Mechanobiology of tendon.* J Biomech, 2006. 39(9): p. 1563-82.

3. Kastelic, J., A. Galeski, and E. Baer, *The multicomposite structure of tendon.* Connect Tissue Res, 1978. 6(1): p. 11-23.

4. Screen, H.R., et al., *An investigation into the effects of the hierarchical structure of tendon fascicles on micromechanical properties.* Proc Inst Mech Eng H, 2004. 218(2): p. 109-19.

5. Cohen, R.E., C.J. Hooley, and N.G. McCrum, *Viscoelastic creep of collagenous tissue.* J Biomech, 1976. 9(4): p. 175-84.

6. Woo, S.L., *Mechanical properties of tendons and ligaments. I. Quasi-static and nonlinear viscoelastic properties.* Biorheology, 1982. 19(3): p. 385-96.

7. Yamamoto, N., et al., *Mechanical properties of the rabbit patellar tendon.* J Biomech Eng, 1992. 114(3): p. 332-7.

8. Johnson, G.A., et al., *Tensile and viscoelastic properties of human patellar tendon.* J Orthop Res, 1994. 12(6): p. 796-803.

9. Duenwald, S.E., R. Vanderby, Jr., and R.S. Lakes, *Viscoelastic relaxation and recovery of tendon.* Ann Biomed Eng, 2009. 37(6): p. 1131-40.

10. Kadler, K.E., A. Hill, and E.G. Canty-Laird, *Collagen fibrillogenesis: fibronectin, integrins, and minor collagens as organizers and nucleators.* Curr Opin Cell Biol, 2008. 20(5): p. 495-501.

11. Holmes, D.F., M.P. Lowe, and J.A. Chapman, *Vertebrate (chick) collagen fibrils formed in vivo can exhibit a reversal in molecular polarity.* J Mol Biol, 1994. 235(1): p. 80-3.

12. Kadler, K.E., et al., *Collagen fibril formation.* Biochem J, 1996. 316 (Pt 1): p. 1-11.

13. Jozsa, L., et al., *Three-dimensional ultrastructure of human tendons.* Acta Anat (Basel), 1991. 142(4): p. 306-12.

14. Kannus, P., *Structure of the tendon connective tissue.* Scand J Med Sci Sports, 2000. 10(6): p. 312-20.

15. Cooper, R.R. and S. Misol, *Tendon and ligament insertion. A light and electron microscopic study.* J Bone Joint Surg Am, 1970. 52(1): p. 1-20.

16. Vanderby, R. and P.P. Provenzano, *Collagen in connective tissue: from tendon to bone.* J Biomech, 2003. 36(10): p. 1523-7.

17. Khoroshkov, Y.A., *Ultrastructural elements of the strength of the muscle-tendon junction.* Mechanics of Composite Materials, 1975. 11(4): p. 535-537.

18. Trotter, J.A., *Structure-function considerations of muscle-tendon junctions.* Comp Biochem Physiol A Mol Integr Physiol, 2002. 133(4): p. 1127-33.

19. Kannus, P., *Structure of the tendon connective tissue.* Scand. Journal of Medicine and Science in Sports, 2000. 10: p. 312-320.

20. Yamamoto, *Mechanical properties of collagen fascicles form the rabbit patellar tendon.* Transactions of the ASME, 1999. 121: p. 124-131.

21. Derwin, K.A. and L.J. Soslowsky, *A quantitative investigation of structure-function relationships in a tendon fascicle model.* J Biomech Eng, 1999. 121(6): p. 598-604.

22. Petruska, J.A. and A.J. Hodge, *A Subunit Model for the Tropocollagen Macromolecule.* Proc Natl Acad Sci U S A, 1964. 51: p. 871-6.

23. Bailey, A.J., *Molecular mechanisms of ageing in connective tissues.* Mech Ageing Dev, 2001. 122(7): p. 735-55.

24. Sasaki, N. and S. Odajima, *Elongation mechanism of collagen fibrils and force-strain relations of tendon at each level of structural hierarchy.* J Biomech, 1996. 29(9): p. 1131-6.

25. Redaelli, A., et al., *Possible role of decorin glycosaminoglycans in fibril to fibril force transfer in relative mature tendons--a computational study from molecular to microstructural level.* J Biomech, 2003. 36(10): p. 1555-69.

26. Barenberg, S.A., F.E. Filisko, and P.H. Geil, *Ultrastructural deformation of collagen.* Connect Tissue Res, 1978. 6(1): p. 25-35.

27. Mosler, E., et al., *Stress-induced molecular rearrangement in tendon collagen.* J Mol Biol, 1985. 182(4): p. 589-96.

28. Kukreti, U. and S.M. Belkoff, *Collagen fibril D-period may change as a function of strain and location in ligament.* J Biomech, 2000. 33(12): p. 1569-74.

29. Prostak, K.S. and S. Lees, *Visualization of crystal-matrix structure. In situ demineralization of mineralized turkey leg tendon and bone.* Calcif Tissue Int, 1996. 59(6): p. 474-9.

30. Yamaguchi, I., et al., *Microstructure analysis of calcium phosphate formed in tendon.* J Mater Sci Mater Med, 2003. 14(10): p. 883-9.

31. Gusnard, D. and R.H. Kirschner, *Cell and organelle shrinkage during preparation for scanning electron microscopy: effects of fixation, dehydration and critical point drying.* J Microsc, 1977. 110(1): p. 51-7.

32. Charulatha, V. and A. Rajaram, *Crosslinking density and resorption of dimethyl suberimidate-treated collagen.* J Biomed Mater Res, 1997. 36(4): p. 478-86.

33. Kjellen, L. and U. Lindahl, *Proteoglycans: structures and interactions.* Annu Rev Biochem, 1991. 60: p. 443-75.

34. Puxkandl, R., et al., *Viscoelastic properties of collagen: synchrotron radiation investigations and structural model.* Philos Trans R Soc Lond B Biol Sci, 2002. 357(1418): p. 191-7.

35. Screen, H.R., et al., *The influence of noncollagenous matrix components on the micromechanical environment of tendon fascicles.* Ann Biomed Eng, 2005. 33(8): p. 1090-9.

36. Robinson, P.S., et al., *Strain-rate sensitive mechanical properties of tendon fascicles from mice with genetically engineered alterations in collagen and decorin.* J Biomech Eng, 2004. 126(2): p. 252-7.

37. Yin, L. and D.M. Elliott, *A biphasic and transversely isotropic mechanical model for tendon: application to mouse tail fascicles in uniaxial tension.* J Biomech, 2004. 37(6): p. 907-16.

38. Elliott, D.M., et al., *Effect of altered matrix proteins on quasilinear viscoelastic properties in transgenic mouse tail tendons.* Ann Biomed Eng, 2003. 31(5): p. 599-605.

39. Weiss, J.A., J.C. Gardiner, and C. Bonifasi-Lista, *Ligament material behavior is nonlinear, viscoelastic and rate-independent under shear loading.* J Biomech, 2002. 35(7): p. 943-50.

40. Liao, J. and I. Vesely, *Skewness angle of interfibrillar proteoglycans increases with applied load on mitral valve chordae tendineae.* J Biomech, 2007. 40(2): p. 390-8.

41. Scott, J.E., *Elasticity in extracellular matrix 'shape modules' of tendon, cartilage, etc. A sliding proteoglycan-filament model.* J Physiol, 2003. 553(Pt 2): p. 335-43.

42. Gandhi, N.S. and R.L. Mancera, *The structure of glycosaminoglycans and their interactions with proteins.* Chem Biol Drug Des, 2008. 72(6): p. 455-82.

43. Vesentini, S., A. Redaelli, and F.M. Montevecchi, *Molecular analysis of interaction energies of the decorin proteoglycan-collagen complex in tendon fibrils*, in *Summer Bioengineering Conference*. 2003: Key Biscayne, Florida.

44. Vesentini, S., A. Redaelli, and F.M. Montevecchi, *Estimation of the binding force of the collagen molecule-decorin core protein complex in collagen fibril.* J Biomech, 2005. 38(3): p. 433-43.

45. Provenzano, P.P. and R. Vanderby, Jr., *Collagen fibril morphology and organization: implications for force transmission in ligament and tendon.* Matrix Biol, 2006. 25(2): p. 71-84.

46. Raspanti, M., T. Congiu, and S. Guizzardi, *Structural aspects of the extracellular matrix of the tendon: an atomic force and scanning electron microscopy study.* Arch Histol Cytol, 2002. 65(1): p. 37-43.

47. Maffulli, N., et al., *Similar histopathological picture in males with Achilles and patellar tendinopathy.* Med Sci Sports Exerc, 2004. 36(9): p. 1470-5.

48. Riley, G., *Chronic tendon pathology: molecular basis and therapeutic implications.* Expert Rev Mol Med, 2005. 7(5): p. 1-25.

49. Bank, R.A., et al., *Lysylhydroxylation and non-reducible crosslinking of human supraspinatus tendon collagen: changes with age and in chronic rotator cuff tendinitis.* Ann Rheum Dis, 1999. 58(1): p. 35-41.

50. Cook, J.L., et al., *A cross sectional study of 100 athletes with jumper's knee managed conservatively and surgically. The Victorian Institute of Sport Tendon Study Group.* Br J Sports Med, 1997. 31(4): p. 332-6.

51. Kongsgaard, M., et al., *Fibril morphology and tendon mechanical properties in patellar tendinopathy: effects of heavy slow resistance training.* Am J Sports Med, 2010. 38(4): p. 749-56.

52. Williams, L.N., et al., *Variation of diameter distribution, number density, and area fraction of fibrils within five areas of the rabbit patellar tendon.* Ann Anat, 2008. 190(5): p. 442-51.

53. Liden, M., et al., *A histological and ultrastructural evaluation of the patellar tendon 10 years after reharvesting its central third.* Am J Sports Med, 2008. 36(4): p. 781-8.

54. Knorzer, E., et al., *New aspects of the etiology of tendon rupture. An analysis of time-resolved dynamic-mechanical measurements using synchrotron radiation.* Arch Orthop Trauma Surg, 1986. 105(2): p. 113-20.

55. Lavagnino, M., et al., *Effect of amplitude and frequency of cyclic tensile strain on the inhibition of MMP-1 mRNA expression in tendon cells: an in vitro study.* Connect Tissue Res, 2003. 44(3-4): p. 181-7.

56. Arnoczky, S.P., et al., *Ex vivo static tensile loading inhibits MMP-1 expression in rat tail tendon cells through a cytoskeletally based mechanotransduction mechanism.* J Orthop Res, 2004. 22(2): p. 328-33.

57. Arnoczky, S.P., M. Lavagnino, and M. Egerbacher, *The mechanobiological aetiopathogenesis of tendinopathy: is it the over-stimulation or the under-stimulation of tendon cells?* Int J Exp Pathol, 2007. 88(4): p. 217-26.

58. Arnoczky, S.P., M. Lavagnino, and M. Egerbacher, *The response of tendon cells to changing loads: Implicatios in the etiopathogenesis of tendinopathy*. Tendinopathy in Athletes: Encyclopaedia of Sports Medicine, ed. S.L. Woo, P. Renstrom, and S.P. Arnoczky. Vol. 12. 2007, Oxford: Blackwell Publishing. 233.

59. Maganaris, C. and M. Narici, *Mechanical Properties of Tendons*, in *Tendon Injuries*. 2005. p. 14-21.

60. Noyes, F.R., et al., *Biomechanical analysis of human ligament grafts used in knee-ligament repairs and reconstructions.* J Bone Joint Surg Am, 1984. 66(3): p. 344-52.

61. Butler, D.L., et al., *On the interpretation of our anterior cruciate ligament data.* Clin Orthop Relat Res, 1985(196): p. 26-34.

62. Woo, S.L., et al., *The effects of strain rate on the properties of the medial collateral ligament in skeletally immature and mature rabbits: a biomechanical and histological study.* J Orthop Res, 1990. 8(5): p. 712-21.

63. Graham, J.S., et al., *Structural changes in human type I collagen fibrils investigated by force spectroscopy.* Exp Cell Res, 2004. 299(2): p. 335-42.

64. Shen, Z.L., et al., *Stress-strain experiments on individual collagen fibrils.* Biophys J, 2008. 95(8): p. 3956-63.

65. Sasaki, N. and S. Odajima, *Stress-strain curve and Young's modulus of a collagen molecule as determined by the X-ray diffraction technique.* J Biomech, 1996. 29(5): p. 655-8.

66. van der Rijt, J.A., et al., *Micromechanical testing of individual collagen fibrils.* Macromol Biosci, 2006. 6(9): p. 697-702.

67. Yang, L., et al., *Mechanical properties of native and cross-linked type I collagen fibrils.* Biophys J, 2008. 94(6): p. 2204-11.

68. Yang, L., et al., *Micromechanical bending of single collagen fibrils using atomic force microscopy.* J Biomed Mater Res A, 2007. 82(1): p. 160-8.

69. Hansen, P., et al., *Glutaraldehyde cross-linking of tendon--mechanical effects at the level of the tendon fascicle and fibril.* Connect Tissue Res, 2009. 50(4): p. 211-22.

70. Folkard, W., et al., *Structural dynamic of native tendon collagen.* J Mol Biol, 1987. 193(2): p. 405-7.

71. Fratzl, P., et al., *Fibrillar structure and mechanical properties of collagen.* J Struct Biol, 1998. 122(1-2): p. 119-22.

72. Liao, J., et al., *Molecular orientation of collagen in intact planar connective tissues under biaxial stretch.* Acta Biomater, 2005. 1(1): p. 45-54.

73. Liao, J., et al., *The relation between collagen fibril kinematics and mechanical properties in the mitral valve anterior leaflet.* J Biomech Eng, 2007. 129(1): p. 78-87.

74. Ackbarow, T. and M.J. Buehler, *Alpha-helical protein domains unify strength and robustness through hierarchical nanostructures.* Nanotechnology, 2009. 20(7): p. 75103.

75. Gautieri, A., M.J. Buehler, and A. Redaelli, *Deformation rate controls elasticity and unfolding pathway of single tropocollagen molecules.* J Mech Behav Biomed Mater, 2009. 2(2): p. 130-7.

76. Chen, C.T., D.S. Malkus, and R. Vanderby, Jr., *A fiber matrix model for interstitial fluid flow and permeability in ligaments and tendons.* Biorheology, 1998. 35(2): p. 103-18.

77. Ciarletta, P. and M. Ben Amar, *A finite dissipative theory of temporary interfibrillar bridges in the extracellular matrix of ligaments and tendons.* J R Soc Interface, 2008.

78. Gupta, H.S., et al., *In situ multi-level analysis of viscoelastic deformation mechanisms in tendon collagen.* J Struct Biol, 2009.

79. Lucas, S.R., et al., *Viscoelastic and failure properties of spine ligament collagen fascicles.* Biomech Model Mechanobiol, 2009.

80. To, S.Y., M.K. Kwan, and S.L. Woo, *Simultaneous measurements of strains on two surfaces of tendons and ligaments.* J Biomech, 1988. 21(6): p. 511-4.

81. Atkinson, T.S., B.J. Ewers, and R.C. Haut, *The tensile and stress relaxation responses of human patellar tendon varies with specimen cross-sectional area.* J Biomech, 1999. 32(9): p. 907-14.

82. Krauss, S., et al., *Inhomogeneous fibril stretching in antler starts after macroscopic yielding: indication for a nanoscale toughening mechanism.* Bone, 2009. 44(6): p. 1105-10.

83. Gupta, H.S., et al., *Nanoscale deformation mechanisms in bone.* Nano Lett, 2005. 5(10): p. 2108-11.

84. Yamamoto, E., et al., *Biomechanical response of collagen fascicles to restressing after stress deprivation during culture.* J Biomech, 2007. 40(9): p. 2063-70.

85. Haut, R.C. and A.C. Powlison, *The effects of test environment and cyclic stretching on the failure properties of human patellar tendons.* J Orthop Res, 1990. 8(4): p. 532-40.

86. Chimich, D., et al., *Water content alters viscoelastic behaviour of the normal adolescent rabbit medial collateral ligament.* J Biomech, 1992. 25(8): p. 831-7.

87. Butler, D.L., M.D. Kay, and D.C. Stouffer, *Comparison of material properties in fascicle-bone units from human patellar tendon and knee ligaments.* J Biomech, 1986. 19(6): p. 425-32.

88. Haraldsson, B.T., et al., *Region-specific mechanical properties of the human patella tendon.* J Appl Physiol, 2005. 98(3): p. 1006-12.

89. Svensson, R.B., et al., *Viscoelastic behavior of discrete human collagen fibrils.* J Mech Behav Biomed Mater. 3(1): p. 112-5.

90. Eppell, S.J., et al., *Nano measurements with micro-devices: mechanical properties of hydrated collagen fibrils.* J R Soc Interface, 2006. 3(6): p. 117-21.

91. Lake, S.P., et al., *Effect of fiber distribution and realignment on the nonlinear and inhomogeneous mechanical properties of human supraspinatus tendon under longitudinal tensile Loading.* J Orthop Res, 2009.

92. Van Sligtenhorst, C., D.S. Cronin, and G. Wayne Brodland, *High strain rate compressive properties of bovine muscle tissue determined using a split Hopkinson bar apparatus.* Journal of Biomechanics, 2006. 39(10): p. 1852-1858.

93. Zhao, H. and G. Gary, *On the use of a viscoelastic split Hopkinson pressure bar.* International Journal of Impact Engineering, 1997. 19(4): p. 319-330.

94. Song, B., et al., *Dynamic and quasi-static compressive response of porcine muscle.* Journal of Biomechanics, 2007. 40(13): p. 2999-3005.

95. Cheng, M., *Mechanical Behavior of Bovine Tendon with Stress-Softening and Loading-Rate Effects.* Adv. Theor. Appl. Mech., 2009. 2(2): p. 59 - 74

96. Chen, J. and L. Priddy, *Mechanical Response of Porcine Liver Tissue under High Strain Rate Compression*. 2010, Mississippi State University: Starkville, MS Unpublished.

97. Prabhu, R. and E. Marin, *Traumatic Brain Injury: Mechanical Response of Porcine Brain Tissue Under High Strain Rate Ttests*. 2010, Center for Advanced Vehicular Systems, Mississippi State University: Starkville, MS Unpublished.

98. Roan, E. and K. Vemaganti, *The nonlinear material properties of liver tissue determined from no-slip uniaxial compression experiments.* Journal of Biomechanical Engineering, 2007. 129: p. 450-456.

99. Saraf, H., et al., *Mechanical properties of soft human tissues under dynamic loading.* Journal of Biomechanics, 2007. 40(9): p. 1960-1967.